X-ray diffraction experiments were performed under cryocooled conditions (100 K) on the BL41XU (λ = 1.000 Å; Rayonix MX225HE CCD detector) and BL44XU (λ = 0.900 Å; Bruker DIP-6040 detector system) beamlines at SPring-8 (Harima, Japan) and the BL17A (λ = 1.000 Å; ADSC Quantum 270 detector) beamline at the Photon Factory (Tsukuba, Japan). A crystal mounted in a nylon loop was transferred to and soaked briefly in reservoir solution containing 40%(*w*/*v*) PEG 400 and then flash-frozen at 100 K in a stream of nitrogen gas. A total of 180 images were recorded with an oscillation angle of 1.0°, an exposure time of 1 s per image and a crystal-to-detector distance of 200 mm. The diffraction data were processed and scaled with the *HKL*-2000 software package (Otwinowski & Minor, 1997).

3. Results and discussion

Gene-sequence analyses for the cDNAs of *T. b. gambiense* and *T. b. rhodesiense gk*s revealed a total of seven point differences when compared with the *gk* sequence from *T. b. brucei* (TREU927; accession No. XM_822408); only one of these differences (T212 in *T. b. brucei* to C in *T. b. gambiense* and *T. b. rhodesiense*) resulted in a change of a single amino acid (Phe71 in TbbGK to Ser71 in TbgGK and TbrGK) in the 512 amino-acid residues of TbgGK. The nucleotide-sequence data for the cDNAs of *T. b. gambiense* and *T. b. rhodesiense gk*s have been deposited in the DDBJ/EMBL/GenBank nucleotide-sequence databases with accession Nos. AB517984 and AB517985, respectively.

His_6-tagged rTbgGK with 545 amino-acid residues (60.4 kDa) was overexpressed and purified to homogeneity by a combination of Ni–NTA affinity chromatography and Superdex 200 gel-filtration chromatography (Fig. 1). About 80 mg purified enzyme with a specific activity of 31.7 µmol min^{-1} mg^{-1} was obtained from a 10 l culture. The rTbgGK protein eluted from the Superdex 200 column with a retention time corresponding to a molecular weight of about 119 kDa, indicating that the enzyme exists as a homodimer in solution.

In a screening of 290 crystallization conditions, crystals of rTbgGK were obtained using PEGs as precipitant. After optimization of the crystallization conditions, the best crystals, which diffracted X-rays to a resolution of 2.75 Å (Fig. 2), were grown at 293 K using a reservoir solution containing 30%(*w*/*v*) PEG 400 and 0.1 *M* HEPES buffer pH 7.0. The crystals attained typical dimensions of about 0.25 × 0.1 × 0.05 mm in 2 d (Fig. 3). Analysis of the symmetry and systematic absences in the recorded diffraction patterns revealed that the crystals of rTbgGK belonged to the orthorhombic space group $P2_12_12_1$, with unit-cell parameters a = 63.84, b = 121.50, c = 154.59 Å. Assuming the presence of two rTbgGK molecules (2 × 60.4 kDa) in the asymmetric unit, the V_M value was calculated to be 2.5 $Å^3$ Da^{-1}, with an estimated solvent content of 50% (Matthews, 1968); these values are within the range commonly observed for protein crystals. A total of 135 987 observed reflections recorded on 180 images were merged to 31 848 unique reflections in the 50.0–2.75 Å resolution range with an R_{merge} of 5.5%. The data-collection and processing statistics are shown in Table 1.

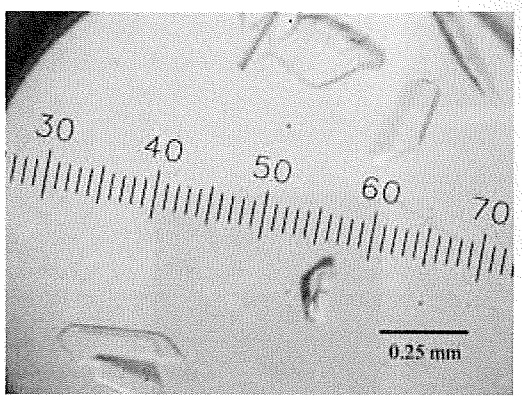

Figure 3
Crystals of rTbgGK obtained by the sitting-drop vapour-diffusion method using PEG 400 as a precipitant.

Table 1
Diffraction data statistics for the crystal of rTbgGK.

Values in parentheses are for the highest resolution shell.

Space group	$P2_12_12_1$
Unit-cell parameters (Å)	a = 63.84, b = 121.50, c = 154.59
V_M† ($Å^3$ Da^{-1})	2.5
Solvent content† (%)	50
X-ray source	BL41XU, SPring8
Wavelength (Å)	1.000
Temperature (K)	100
Resolution (Å)	50–2.75 (2.85–2.75)
Total reflections	135987
Unique reflections	31848
Completeness (%)	97.1 (95.7)
$R_{merge}(I)$‡ (%)	5.5 (46.1)
$\langle I/\sigma(I)\rangle$	18.4 (3.0)

† Assuming the presence of two molecules in the asymmetric unit. ‡ $R_{merge}(I) = \sum_{hkl}\sum_i |I_i(hkl) - \langle I(hkl)\rangle| / \sum_{hkl}\sum_i I_i(hkl)$, where $I_i(hkl)$ is the intensity of the ith observation of reflection hkl and $\langle I(hkl)\rangle$ is their average.

An attempt to solve the structure using the molecular-replacement method with the *MOLREP* program (Vagin & Teplyakov, 1997) from the *CCP*4 suite (Collaborative Computational Project, Number 4, 1994) was carried out using the refined coordinates of GK from *P. falciparum* (PDB code 2w41; 40% amino-acid sequence identity to rTbgGK; Schnick *et al.*, 2009). A promising solution with a homodimeric structure was obtained (correlation coefficient and R factor of 0.406 and 51.6%, respectively). Using the molecular-replacement solution, the structure is being subjected to refinement. In parallel with the refinement, we are now trying to obtain crystals of rTbgGK complexed with ligands, including substrates and substrate analogues. *In silico* screening of potential inhibitors from a compound library of the Chemical Biology Research Initiative at the University of Tokyo is also under way.

It should be noted that the amino-acid sequence of TbgGK was identical to that of TbrGK and showed only one difference from that of TbbGK. Therefore, inhibitors of TbgGK should also be effective against other trypanosome GKs. Since TbgGK provides a greater potential as the primary target of chemotherapy, detailed structures of TbgGK complexed with inhibitors will help structure-based drug design aimed at African trypanosomiasis.

We thank all the staff members of beamlines BL41XU and BL44XU at SPring-8 and BL17A at the Photon Factory for their help with the X-ray diffraction experiments. This work was supported by a grant from the Targeted Proteins Research Program (TPRP) and was supported in part by a Grant-in-Aid for Creative Scientific Research (18GS0314 to KK) from the Japan Society for the Promotion of Science and a Grant-in-Aid for Scientific Research on Priority Areas (18073004 to KK) from the Ministry of Education, Culture, Sports, Science and Technology, Japan. EOB is supported by a Japanese

Government Scholarship from the Ministry of Education, Science, Culture, Sports, Science and Technology.

References

Brun, R., Schumacher, R., Schmid, C., Kunz, C. & Burri, C. (2001). *Trop. Med. Int. Health*, **6**, 906–914.

Chaudhuri, M., Ott, R. D. & Hill, G. C. (2006). *Trends Parasitol.* **22**, 484–491.

Colasante, C., Ellis, M., Ruppert, T. & Voncken, F. (2006). *Proteomics*, **6**, 3275–3293.

Collaborative Computational Project, Number 4 (1994). *Acta Cryst.* D**50**, 760–763.

Fairlamb, A. H., Opperdoes, F. R. & Borst, P. (1977). *Nature (London)*, **265**, 270–271.

Guerra, D. G., Decottignies, A., Bakker, B. M. & Michels, P. A. (2006). *Mol. Biochem. Parasitol.* **149**, 155–169.

Haanstra, J. R., van Tuijl, A., Kessler, P., Reijnders, W., Michels, P. A., Westerhoff, H. V., Parsons, M. & Bakker, B. M. (2008). *Proc. Natl Acad. Sci. USA*, **105**, 17718–17723.

Hannaert, V., Bringaud, F., Opperdoes, F. R. & Michels, P. A. (2003). *Kinetoplastid Biol. Dis.* **2**, 1–30.

Hurley, J. H. (1996). *Annu. Rev. Biophys. Biomol. Struct.* **25**, 137–162.

Kido, Y., Shiba, T., Inaoka, D. K., Sakamoto, K., Nara, T., Aoki, T., Honma, T., Tanaka, A., Inoue, M., Matsuoka, S., Moore, A., Harada, S. & Kita, K. (2010). *Acta Cryst.* F**66**, 275–278.

Kralova, I., Rigden, D. J., Opperdoes, F. R. & Michels, P. A. (2000). *Eur. J. Biochem.* **267**, 2323–2333.

Laemmli, U. K. (1970). *Nature (London)*, **227**, 680–685.

Matthews, B. W. (1968). *J. Mol. Biol.* **33**, 491–497.

Michels, P. A., Hannaert, V. & Bringaud, F. (2000). *Parasitol. Today*, **16**, 482–489.

Minagawa, N., Yabu, Y., Kita, K., Nagai, K., Ohta, N., Meguro, K., Sakajo, S. & Yoshimoto, A. (1997). *Mol. Biochem. Parasitol.* **84**, 271–280.

Njiokou, F., Laveissière, C., Simo, G., Nkinin, S., Grébaut, P., Cuny, G. & Herder, S. (2006). *Infect. Genet. Evol.* **6**, 147–153.

Njogu, R. M., Whittaker, C. J. & Hill, G. C. (1980). *Mol. Biochem. Parasitol.* **1**, 13–29.

Otwinowski, Z. & Minor, W. (1997). *Methods Enzymol.* **276**, 307–326.

Schnick, C., Polley, S. D., Fivelman, Q. L., Ranford-Cartwright, L. C., Wilkinson, S. R., Brannigan, J. A., Wilkinson, A. J. & Baker, D. A. (2009). *Mol. Microbiol.* **71**, 533–545.

Singha, U. K., Peprah, E., Williams, S., Walker, R., Saha, L. & Chaudhuri, M. (2008). *Mol. Biochem. Parasitol.* **159**, 30–43.

Stevens, J. R. & Brisse, S. (2004). *The Trypanosomiases*, edited by I. Maudlin, P. Holmes & M. Miles, pp. 1–23. Wallingford: CAB International.

Van Der Meer, C. & Versluijs-Broers, J. A. (1979). *Exp. Parasitol.* **48**, 126–134.

Vagin, A. & Teplyakov, A. (1997). *J. Appl. Cryst.* **30**, 1022–1025.

World Health Organization (2006). *African trypanosomiasis*. http://www.who.int/mediacentre/factsheets/fs259/en/.

Yabu, Y., Suzuki, T., Nihei, C., Minagawa, N., Hosokawa, T., Nagai, K., Kita, K. & Ohta, N. (2006). *Parasitol. Int.* **55**, 39–43.

Biochimica et Biophysica Acta 1797 (2010) 443–450

Contents lists available at ScienceDirect

Biochimica et Biophysica Acta

journal homepage: www.elsevier.com/locate/bbabio

Purification and kinetic characterization of recombinant alternative oxidase from *Trypanosoma brucei brucei*

Yasutoshi Kido [a], Kimitoshi Sakamoto [a], Kosuke Nakamura [a], Michiyo Harada [a], Takashi Suzuki [b], Yoshisada Yabu [b], Hiroyuki Saimoto [c], Fumiyuki Yamakura [d], Daijiro Ohmori [d], Anthony Moore [e], Shigeharu Harada [f], Kiyoshi Kita [a,*]

[a] *Department of Biomedical Chemistry, Graduate School of Medicine, The University of Tokyo, Tokyo 113-0033, Japan*
[b] *Department of Molecular Parasitology, Graduate School of Medical Sciences, Nagoya City University, Nagoya 467-8601, Japan*
[c] *Department of Materials Science, Faculty of Engineering, Tottori University, Tottori, Japan*
[d] *Department of Chemistry, School of Medicine, Juntendo University, Tokyo, Japan*
[e] *Biochemistry and Biomedical Sciences, School of Life Sciences, University of Sussex, Falmer, Brighton, UK*
[f] *Department of Applied Biology, Graduate School of Science and Technology, Kyoto Institute of Technology, Kyoto 606-8585, Japan*

ARTICLE INFO

Article history:
Received 24 September 2009
Received in revised form 23 December 2009
Accepted 25 December 2009
Available online 4 January 2010

Keywords:
Alternative oxidase
Membrane-bound diiron protein
Trypanosoma brucei
Ascofuranone
Chemotherapy

ABSTRACT

The trypanosome alternative oxidase (TAO) functions in the African trypanosomes as a cytochrome-independent terminal oxidase, which is essential for their survival in the mammalian host and as it does not exist in the mammalian host is considered to be a promising drug target for the treatment of trypanosomiasis. In the present study, recombinant TAO (rTAO) overexpressed in a haem-deficient *Escherichia coli* strain has been solubilized from *E. coli* membranes and purified to homogeneity in a stable and highly active form. Analysis of bound iron detected by inductively coupled plasma-mass spectrometer (ICP-MS) reveals a stoichiometry of two bound iron atoms per monomer of rTAO. Confirmation that the rTAO was indeed a diiron protein was obtained by EPR analysis which revealed a signal, in the reduced forms of rTAO, with a g-value of 15. The kinetics of ubiquiol-1 oxidation by purified rTAO showed typical Michaelis–Menten kinetics (K_m of 338 μM and V_{max} of 601 μmol/min/mg), whereas ubiquinol-2 oxidation showed unusual substrate inhibition. The specific inhibitor, ascofuranone, inhibited the enzyme in a mixed-type inhibition manner with respect to ubiquinol-1.

1. Introduction

Trypanosoma brucei is a parasite that causes African sleeping sickness in humans and Nagana in livestock and is transmitted by the tsetse fly. There is an urgent need for further development of chemotherapy against African trypanosomiasis since current chemotherapeutic drugs are not entirely satisfactory [1].

Trypanosomal parasites are equipped with a unique energy metabolism, they live as the bloodstream form in the mammalian host and as the procyclic form in the vector. The procyclic form of *T. brucei* fulfills its ATP requirement from a cyanide-sensitive and cytochrome-dependent respiratory chain comparable to that observed in the host mitochondria, whereas in the bloodstream form, trypanosomes use the glycolytic pathway, which is localized in a unique organelle the glycosome, as their major source of ATP [2–5]. Once the parasites invade the mammalian host in the bloodstream form, both its cytochrome-dependent respiratory chain and ATP synthesis by oxidative phosphorylation disappear [2,5]. Instead a cyanide-resistant and cytochrome-independent trypanosomal alternative oxidase (TAO) functions as the sole terminal oxidase to re-oxidize NADH accumulated during glycolysis [5].

TAO is generally considered to be a good target for the anti-trypanosomal drugs because this oxidase is essential for their survival, since it reoxidises cytosolic NADH, and mammalian hosts do not possess this protein [5,6]. Indeed, we found that ascofuranone, isolated from the pathogenic fungus *Ascochyta visiae*, specifically inhibits the quinol oxidase activity of TAO and rapidly kills the parasites [7]. In addition, we have confirmed the chemotherapeutic efficacy of ascofuranone *in vivo* [8,9].

The alternative oxidase (AOX) is a non-protonmotive ubiquinol oxido-reductase catalyzing the 4-electron reduction of dioxygen to water [5,10–12]. Genes encoding AOX have been found in higher

Abbreviations: AOX, alternative oxidase; DM, *n*-dodecyl-β-D-maltopyranoside; EPR, electron paramagnetic resonance; ICP-MS, inductively coupled plasma-mass spectrometer; IPTG, isopropyl, β-D-1-thiogalactoside; k_{cat}, molecular activity; C10E8, octaethylene glycol-monododecylether; OG, *n*-octyl-β-D-glucopyranoside; rTAO, recombinant trypanosome alternative oxidase; SHAM, salycylhydroxamic acid; TAO, trypanosome alternative oxidase; Ubiquinol, reduced form ubiquinone

* Corresponding author. Department of Biomedical Chemistry, Graduate School of Medicine, The University of Tokyo, Hongo, Bunkyo-ku, Tokyo 113-0033, Japan. Tel.: +81 3 5841 3526; fax: +81 3 5841 3444.
E-mail address: kitak@m.u-tokyo.ac.jp (K. Kita).

0005-2728/$ – see front matter © 2009 Elsevier B.V. All rights reserved.
doi:10.1016/j.bbabio.2009.12.021

plants, algae, yeast, slime molds, free-living amoebae, eubacteria and nematodes [13–16]. Moreover, recent bioinformatic searches have broadened the taxonomic distribution of AOX to some members of the animal kingdom [17]. The primary role of AOX in non-thermogenic plants is to regulate cellular redox balance and to protect against reactive oxygen species particularly when the cytochrome pathway is inhibited [18–20]. In addition to this role, many other physiological roles have been described for AOXs in other organisms and these have been discussed in detail elsewhere [13,21]. The ubiquitous occurrence of AOX may suggest that the metabolic flexibility that the alternative pathway confers upon an organism allows it to respond to a wide range of developmental and environmental conditions [22].

Despite universal conservation of the gene and diversified physiology, the molecular features of AOX have not yet been well characterized. Although no high-resolution AOX structure has been determined to date, current structural models predict that it is an integral interfacial membrane protein that interacts with a single leaflet of the lipid bilayer, and contains a non-haem diiron carboxylate active site [23,24]. This model is supported by extensive site-directed mutagenesis studies [18,25–29] and furthermore both EPR and FTIR spectroscopies have confirmed the presence of a binuclear iron center in both the plant and trypanosomal enzymes [30–32].

Further detailed structural and biochemical analyses of AOXs, however, requires further development of purification protocols to produce sufficiently purified and highly active protein to enable crystallization trials and kinetic analyses to proceed. In this paper, we report on the further refinement of our previous protocol through over-expressing rTAO in an *E. coli ΔhemA* mutant (FN102) strain, which lacks quinol oxidase activity of cytochrome *bo* and *bd* complexes [33–35]. Purified rTAO protein is highly active and exhibits an exceptional stability upon storage. The analysis of the prosthetic groups by inductively coupled plasma-mass spectrometer (ICP-MS) and electron paramagnetic resonance (EPR) reveals the presence of two ferric ions stoichiometrically bound per rTAO monomer. To our knowledge this is the first direct confirmation of two ferric irons per AOX. Furthermore we show that purified rTAO is potently inhibited by ascofuranone with mixed function kinetics.

2. Materials and methods

2.1. Preparation of membrane sample

The strain FN102/pTbAO carrying cDNA for *T. b. brucei* TAO [36] was pre-cultured at 37 °C in 100 ml of LB medium containing 10 mg ampicillin, 5 mg kanamycin, and 5 mg 5-aminolevulinic acid for 4–6 h. The pre-cultured cells were aerobically grown at 30 °C in 10 l of S-medium containing 100 g tryptone peptone, 50 g yeast extract, 50 g casamino acid, 104 g K_2HPO_4, 30 g KH_2PO_4, 7.5 g trisodium-citrate·$2H_2O$, 25 g $(NH_4)_2SO_4$, 0.5 g $MgSO_4 \cdot 7H_2O$, 0.25 g $FeSO_4 \cdot 7H_2O$, 0.25 g $FeCl_3$, 0.2%(w/v) glucose, and 1 g carbenicillin. The culture was initiated at O.D.$_{600}$ = 0.01 and expression of rTAO was induced by the addition of isopropyl β-D-1-thiogalactoside (IPTG) (25 μM) at O.D.$_{600}$ = 0.1. Cells were harvested 8–10 h following induction and were resuspended in 50 mM Tris–HCl (pH 7.5) containing 20%(w/w) sucrose, 0.1 mM phenylmethane sulfonyl fluoride (PMSF) and protease inhibitor cocktail (Sigma) and broken by a French Pressure Cell (Ohtake, Tokyo). Unbroken cells were removed by centrifugation at 8000 *g* for 10 min (Hitachi 21G). Inner membranes of FN102/pTbAO were fractionated in high density sucrose after ultracentrifugation at 200,000 *g* for 1 h at 4 °C (Hitachi 85H) (35 ml of supernatant was overlaid over 35 ml of 50 mM Tris–HCl pH 7.5 containing 40%(w/w) sucrose per ultracentrifuge tube). Buoyant inner rich membranes upon 40%(w/w) sucrose layer were fractionated and the inner membrane pellet was separated by further ultracentrifugation at 200,000 *g* for 1 h (HITACHI 85H). The membrane pellet was resuspended in 50 mM Tris–HCl (pH 7.5) containing 20%(w/w) sucrose.

2.2. Solubilization

Membranes were treated with solubilization buffer (6 mg/ml protein in 50 mM Tris–HCl, 1.4%(w/v) *n*-octyl-β-D-glucopyranoside (OG), 200 mM $MgSO_4$, 20%(v/v) glycerol, pH 7.3) at 4 °C and immediately ultracentrifuged at 200,000 *g* for 1 h at 4 °C. The quinol oxidase activities of the samples before centrifugation, as well as that of supernatant and pellet were determined.

2.3. Purification of rTAO

Hybrid batch/column procedure described in the manufacturer's instruction was used as stated below. Ten milliliter of the resin (BD Bioscience, TALON Metal Affinity Resin) was equilibrated in a batch format by 100 ml of equilibration buffer (20 mM Tris–HCl, 1.4%(w/v) OG, 100 mM $MgSO_4$, 20%(v/v) glycerol, pH 7.3). Twenty milliliter of OG extract was mixed with the resin for 20 min at 4 °C. The resin was washed twice with 100 ml of wash buffer (20 mM Tris–HCl, 20 mM imidazole, 0.042%(w/v) *n*-dodecyl-β-D-maltopyranoside (DM), 50 mM $MgSO_4$, 20%(v/v) glycerol pH 7.3) and the resin bound rTAO was transferred to a column for additional washing with 20 ml of second wash buffer (20 mM Tris–HCl, 165 mM imidazole, 0.042%(w/v) DM, 50 mM $MgSO_4$, 20%(v/v) glycerol pH 7.3; flow rate 1 ml/min) and protein elution. Finally, rTAO was eluted with elution buffer (20 mM Tris–HCl, 200 mM imidazole, 0.042%(w/v) DM, 50 mM $MgSO_4$, 60 mM NaCl, 20%(v/v) glycerol pH 7.3; flow rate 1 ml/min). Fractions (4 ml each) were collected.

2.4. Quantitative analysis of metals and EPR spectroscopy

Three independent preparations of rTAO were analyzed (details in Section 3). Each sample solution containing 0.1 g of rTAO was added to 1 ml of nitric acid and 7 ml of water. Organic compounds were hydrolyzed by microwave-assisted protein digestion system (Ethos Pro, Milestone General). Fe, Mn, Cu, Zn and Co in each sample were quantified by inductively coupled plasma-mass spectrometer (ICP-MS, ELAN DRC PerkinElmer Japan). Analysis was performed by the Sumika Chemical Analysis Center (Osaka, Japan). Protein concentration was determined by the Lowry method.

EPR spectra were recorded on a JEOL X-band JES-FA300 spectrometer equipped with an ES-CT470 Heli-Tran cryostat system and a Scientific Instruments digital temperature indicator/controller model 9700a. For EPR analysis of rTAO, 13 mg/ml purified rTAO was frozen in EPR tubes in liquid nitrogen. The purified rTAO was reduced by 2 mM dithionite and 1 mM phenazine methosulfate prior to freezing.

2.5. Ubiquinol oxidase assay

Ubiquinol oxidase activity was measured by recording the absorbance change of ubiquinol-1 at 278 nm (Shimadzu spectrophotometer UV-3000). Reactions were started by the addition of ubiquinol-1 (final concentration 150 μM, $\varepsilon_{278} = 15{,}000\ M^{-1}\ cm^{-1}$) after 2 min preincubation at 25 °C in the presence of rTAO and 50 mM Tris–HCl (pH 7.4). For the enzyme kinetics of purified rTAO, the reaction was initiated by the addition of ubiquinol-1 after 2 min preincubation at 25 °C in the presence of rTAO and 50 mM Tris–HCl (pH 7.4) containing 0.05%(w/v) octaethylene glycol-monododecylether detergent (C10E8).

2.6. Chemicals

All chemicals were biochemistry grade. Ubiquinone-1 and protease inhibitor cocktail were purchased from Sigma-Aldrich. The other detergents were purchased from Dojin Chemicals (Tokyo, Japan).

3. Results

3.1. Purification of fully active TAO

Although we previously established a protocol for the overproduction of rTAO in *E. coli* FN102 (*ΔhemA*) lacking cytochrome *bo* and *bd* complexes of the bacteria, the yield of the active enzyme was too low to analyze its prosthetic group [36]. Such a preparation also hampered the determination of kinetic parameters of rTAO such as its molecular activity. Therefore, conditions for the expression of rTAO and purification protocols were optimized to obtain large quantities of active and stable rTAO to enable such determinations. Three factors were critical to obtain large amounts of active rTAO, namely, growth time of the culture prior to addition of IPTG, absolute concentration of IPTG, and the use of purified inner membranes as the starting material.

After extensive screening of detergents and additives to establish the procedure for efficient extraction of active rTAO from the inner membranes, we found that *n*-octyl-β-D-glucopyranoside (OG) specifically solubilized rTAO as shown in Table 1 (specific activity increased from 23.3 to 63.2 μmol/min/mg after solubilization). Approximately 60% of the membrane quinol oxidase activity was recovered with 1.4%(w/v) OG in the extract (Sup. Fig. 1). Thus, recovery of the activity was significantly higher than that of previously reported digitonin extraction (17%) [36]. Following solubilization, it was possible to maintain enzymatic activity for at least 1 month at 20 °C.

Since rTAO was fused with N-terminal histidine tag, solubilized rTAO was purified by cobalt affinity chromatography. Although the enzyme solubilized by OG was bound to the cobalt affinity resin in the presence of OG, it was not possible to elute bound rTAO from the resin with buffer containing OG. Interestingly, however, we found that 100% of the rTAO activity could be recovered from the column when OG in the washing and elution buffers was exchanged with *n*-dodecyl-β-D-maltopyranoside (DM). In the final step, purified rTAO was obtained by a two-step elution with 165 mM and 200 mM imidazole, which resulted in a very efficient purification of active rTAO in the presence of DM. A typical elution profile of quinol oxidase activity with increasing imidazole concentration is shown in Sup. Fig. 1B. Purified rTAO, with a molecular mass of 34 kDa, was estimated to be 95% pure by SDS-PAGE (Fig. 1A, lane 5). In addition to the 34 kDa band, it is apparent that other bands are also present including two with a smaller size than rTAO and one band with an approximate molecular mass of 74 kDa. Since all of these bands were recognized in Western blot using a monoclonal antibody against TAO (Fig. 1B), the smaller protein bands possibly represent proteolytic breakdown products whilst the 74 kDa band most likely represents the dimeric form of rTAO. The specific activity of purified rTAO was more than 200 μmol/min/mg protein when 150 μM of ubiquinol-1 was used as a substrate, which had a five-fold higher activity than that of the previously purified rTAO (approximately 40 μmol/min/mg) [36]. Quinol oxidase activity of purified rTAO was insensitive to 5 mM KCN but was completely inhibited by 10 nM ascofuranone. A greater than 35-fold increase in purification was achieved using the techniques described above, and 13.2% of the total activity was recovered from the lysate of FN102/pTAO cells as summarized in Table 1. Such procedures resulted in approximately 10 mg of highly purified rTAO from a 10 l culture.

Table 1
Purification of rTAO.

Fractions	Total activity (μmol/min)	Protein (mg)	Specific activity (μmol/min/mg)	Recovery (%)
E. coli lysate	14100	2410	5.85	100
Inner membrane	3500	150	23.3	24.8
OG extract	2400	37.9	63.2	17.0
Co-column	1860	8.95	207	13.2

The activities listed here were measured using 150 μM of ubiquinol-1. Fractions (eluate numbers 6–13 in Supplemental Fig. 1B) were collected as purified rTAO after co-column.

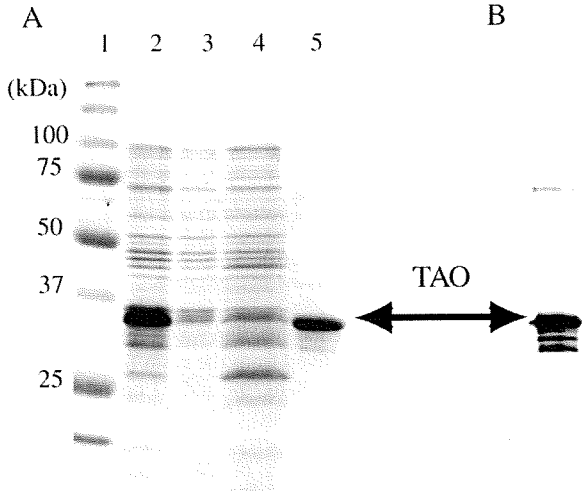

Fig. 1. SDS-PAGE and Western blotting of rTAO in purification steps. A: CBB-staining 12.5% SDS-PAGE of each fraction from the cobalt column chromatography. Lane 1, marker; lanes 2 and 3, each 5 ml of OG extract and flow through fraction; lane 4, 500 ml of wash fraction; and lane 5, 60 ml of eluted fraction collected from fractions 6–12. Loading samples on lanes 2 to 5 were precipitated with acetone. B: Western blot of purified rTAO. The same sample to lane 5 in panel B was electrophoresed on 12.5% polyacrylamide gel. Monoclonal antibodies were used against highly purified rTAO obtained by a nickel column in the presence of guanidine. Epitope recognized by this antibody is the C-terminal domain of the enzyme. The arrow indicates rTAO with an apparent molecular mass of 34 kDa.

3.2. Iron content in purified TAO

Since a highly active and stable purified rTAO could be obtained by the protocol described above, the metal content of purified rTAO was measured by ICP-MS. On the basis that TAO has a diiron center as previously proposed [23,24], then two equivalents of iron should be detected per monomer of rTAO. To this end we analyzed the iron content of purified native rTAO, inactive rTAO, denatured rTAO, and iron within the buffer eluted from the cobalt-column. Purified native rTAOs derived from three independent *E. coli* cultures were precipitated by PEG 3350 and resuspended in the elution buffer at three different concentrations as shown in Sup. Table 1. To prepare inactive rTAO, precipitated rTAO was resuspended in 50 mM Tris–HCl pH 7.4, which resulted in complete loss of enzyme activity. Denatured rTAO was prepared by resuspending the precipitant in elution buffer containing 6 M guanidine–HCl and 0.3 M EDTA. Metal contents in these preparations were 9000 ng/ml, 2900 ng/ml and 1800 ng/ml of Fe respectively for the native rTAO (3.71, 1.19 and 0.80 mg/ml), 230 ng/ml, 100 ng/ml and 28 ng/ml of Fe for inactive rTAO, denatured rTAO and the elution buffer, respectively (Sup. Table 1). From these results, the stoichiometry of bound iron per rTAO monomer can be deduced as indicated below, based on the following parameters namely, a molecular mass of rTAO of 39,391 Da (including the 6× histidine tag), purity of 95% based on SDS-PAGE gels, and the atomic weight of Fe being 55.85. Thus the ratio of iron atoms per rTAO is 1.76 for native rTAO and 0.2 and 0.08 in inactive rTAO and denatured rTAO, respectively (Table 2). This data indicates that one monomer of TAO possesses two atoms of iron which are released during inactivation or denaturation of the enzyme. To our knowledge, this is the first direct measurement of iron in purified AOX and the stoichiometry is consistent with the active site of AOX being a diiron carboxylate-center.

Other metals including Mn, Cu and Zn were also analyzed (Sup. Table 1). In all cases, these metals were below their detection limit (10 ng/ml sample solution) or background level. Although cobalt was

Table 2
Ratio of metals to purified rTAO.

	Fe/rTAO	Zn/rTAO	Mn/rTAO	Cu/rTAO
	Mean ± S.D.			
Native rTAO	1.76 ± 0.077	0.03 ± 0.013	N.D.[a]	N.D.
Inactive rTAO	0.22[b]	N.D.	N.D.	N.D.
Denatured rTAO	0.08[b]	N.D.	N.D.	N.D.

Stoichiometric ratio of metals to one molecular TAO was calculated using data in Supplemental Table 1.
[a] N.D. represents Not Detected (below 0.01).
[b] The value is an average of two independent experiments.

detected in purified rTAO, its concentration was comparable to that of cobalt in the elution buffer derived from the resin (data not shown). Similarly although 130 ng/ml, 66 ng/ml and 61 ng/ml of Zn were detected in native rTAO, these amounts of Zn were not commensurate with that of the enzyme stoichiometry. The detected Zn might be derived from the Zn-substituted form of rTAO, which was suggested to be possible from structural analysis [37]. In addition, at least 90% of the purified rTAO retained its prosthetic group in its active form.

In addition to measuring the stoichiometry of iron in purified rTAO, EPR analysis of purified rTAO was also performed in order to confirm that purified rTAO was indeed a diiron carboxylate protein and whether the detected iron originated from a diiron binding center. As shown in Fig. 2, a low field EPR signal at approximately $g = 15$ in the perpendicular EPR mode was observed with the reduced form of rTAO when the enzyme was reduced by 2 mM of dithionite and 1 mM of phenazine methosulfate (PMS), although the intensity of the signal was low. Importantly the signal disappeared in the oxidized form of rTAO. This low field EPR signal is characteristic for diiron proteins and is ascribed to an exchange-coupled high spin ferrous iron [38]. Although this signal is not normally observed in the perpendicular mode, it can be detected under certain conditions as outlined in this report [39]. The effective g-value of 15 observed in the perpendicular mode is slightly lower than the value of 16 previously observed by us [31] but this is probably due to the fact that parallel-mode EPR spectroscopy is a much more sensitive probe than the perpendicular mode. Nevertheless the finding of a low field signal when the purified enzyme is reduced is further confirmation that the purified rTAO we report here is indeed a diiron carboxylate protein. It should be noted however that we were unable to observe the $g = 15$ signal when the enzyme was reduced by more physiological reductants such as ubiquinol-1 the reasons for which are, at present, unclear.

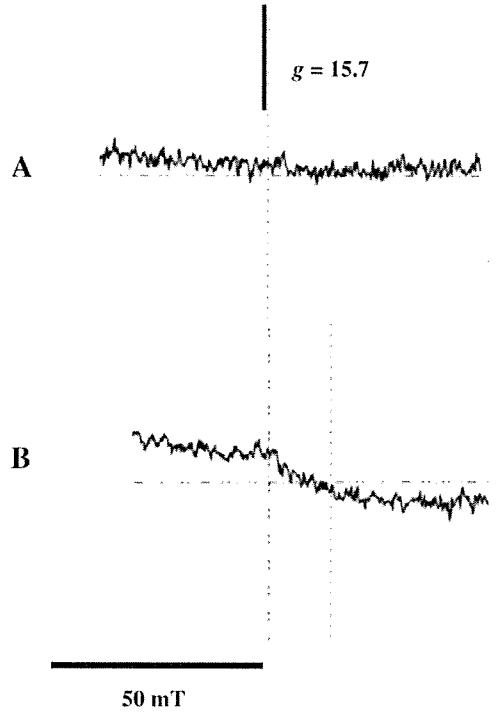

Fig. 2. EPR spectra of rTAO. A: Oxidized form of rTAO (360 μM). B: Reduced form of rTAO (360 μM), which was treated by 2 mM of dithionite and 1 mM phenazine methosulfate for 30 min on ice. Instrument parameters: microwave frequency, 9.02 GHz; microwave power, 1 mW; modulation frequency, 100 kHz; modulation amplitude, 0.6 mT; and temperature of 5 K.

3.3. Kinetic properties of purified TAO

Kinetic analysis of purified rTAO (or AOX) using ubiquinone analogs has previously proved difficult because: 1) the enzyme, following solubilization, was extremely unstable, 2) the natural substrate of trypanosome AOX is ubiquinol-9 [4], which is too hydrophobic to use as the substrate in the assay and 3) the enzymatic activity was not saturated at the maximum concentration of ubiquinol-1 (approximately 300 μM). Since we have purified rTAO in a fully active form and confirmed the stoichiometric presence of the diiron center, the purified rTAO was well-suited to a kinetic analysis.

As noted in our earlier study [36] and in AOXs from other organisms [40] non Michaelis–Menten kinetics is observed when ubiquinol-1 is used as a substrate. Hoefnagel et al. [40], however, observed that the addition of a specific detergent (0.025% EDT-20) during the assay increased the activity by 3- to 4-fold close to saturation. Although the addition of 0.025%(w/v) of EDT-20 equally enhanced the activity of purified rTAO by approximately 2-fold, it did have a deleterious effect upon the long term stability of the enzyme (Sup. Fig. 2).

In an attempt to overcome this problem, various detergents were therefore screened to determine if they could enhance activity without affecting enzyme stability. When the effect of the detergents on enzyme activity was evaluated by monitoring the activity of rTAO in the presence of detergent (Sup. Fig. 3), most activity was retained in the presence of 0.05%(w/v) of C10E8 (Sup. Fig. 4A). Light scattering at 400 nm confirmed that at least 600 μM of ubiquinol-1 was soluble in the assay system (Sup. Fig. 4B). The kinetics of ubiquinol-1 oxidation by purified rTAO in the presence of 0.05%(w/v) of C10E8 showed typical Michaelis–Menten kinetics (Fig. 3, K_m of 338 ± 23.2 μM and V_{max} of 601 ± 27.0 μmol/min/mg). In contrast, activity was linearly dependent upon substrate concentration in the absence of detergent indicating unsaturation in agreement with previous studies [36,40] (Fig. 4). Enzymatic analysis was performed with a wide range of

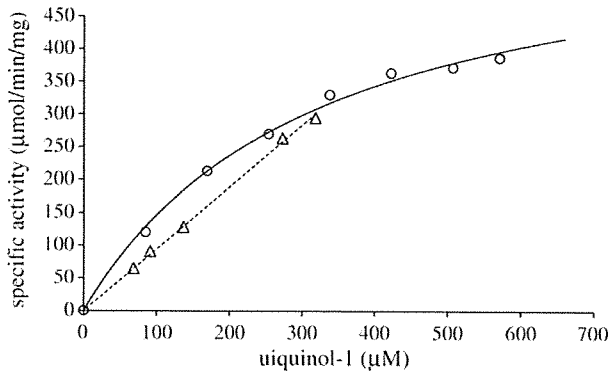

Fig. 3. Kinetics of ubiquinol-1 oxidation by purified rTAO. S–V plot of ubiquinol oxidase activity is shown using 75 ng of purified rTAO in 50 mM Tris–HCl (pH 7.4) and ubiquinol-1 (80–580 μM) with (○) and without (△) 0.05%(w/v) C10E8 at 25 °C. The solid line indicates the fitted Michaelis–Menten kinetics with the detergent (K_m of 338 ± 23.2 μM and V_{max} of 601 ± 27.0 μmol/min/mg), whereas the dashed line indicates the linear relationship between the substrate concentration and the activity without the detergent.

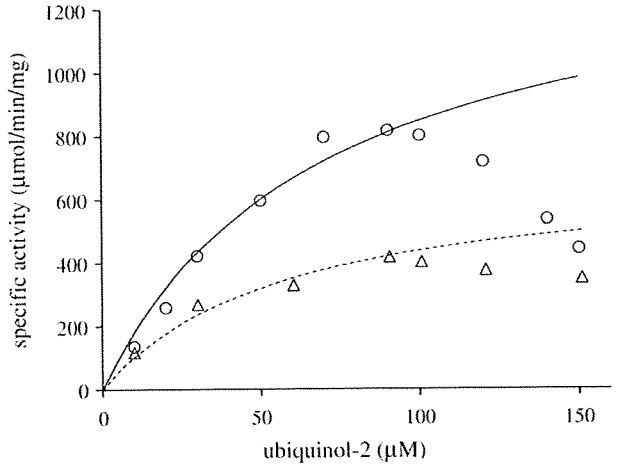

Fig. 4. Kinetics of ubiquinol-2 oxidation by purified rTAO. S–V plot of ubiquinol oxidase activity is shown using 75 ng of purified rTAO in 50 mM Tris–HCl (pH 7.4) and ubiquinol-2 (10–150 μM) with (△) 0.05%(w/v) C10E8 and with (○) 0.025%(w/v) EDT-20 at 25 °C. The solid line indicates the fitted Michaelis–Menten kinetics in the concentration range below 90 μM of ubiquinol-2 with 0.025%(w/v) EDT-20, whereas the dashed line does with 0.05%(w/v) C10E8 (K_m of 71 ± 1.2 μM and V_{max} of 1,460 ± 53.2 μmol/min/mg with 0.025%(w/v) EDT-20, whereas K_m of 57 ± 8.5 μM and V_{max} of 691 ± 28.0 μmol/min/mg with 0.05%(w/v) C10E8).

substrate concentrations (80–570 μM), which corresponded to 0.4 K_m–1.7 K_m.

To investigate whether the length of the side chain of the substrate affected the kinetic properties of rTAO, a kinetic analysis using ubiquinol-2 in the presence of EDT-20 and C10E8 (Fig. 4) was performed. Fig. 4 indicates that during the oxidation of ubiquinol-2, enzyme activity decreased above 100 μM substrate even in buffers containing either detergent. Although kinetic parameters using ubiquinol-2 could not be obtained due to substrate inhibition, S–V plots in the concentration range below 90 μM of ubiquinol-2 could be used to qualitatively analyze the effects of side chain on enzyme activity. Calculated values from such plots revealed that in the presence of 0.025%(w/v) EDT-20 the K_m (ubiquinol-2) was 71 ± 1.2 μM and V_{max} = 1460 ± 53.2 μmol/min/mg whereas with, 0.05%(w/v) C10E8 the K_m was 57 ± 8.5 μM and V_{max} = 691 ± 28.0 μmol/min/mg.

Ascofuranone is a highly specific and potent inhibitor of TAO [7] and it was therefore of importance to determine its inhibitory effect on ubiquinol-1 oxidation by purified rTAO in the presence of 0.05%(w/v) of C10E8 (Sup. Fig. 5A). From the data presented in Sup. Fig. 5A the apparent kinetic parameters of ubiquinol-1 oxidation in the presence of 0.5 nM and 2 nM of ascofuranone were estimated to be respectively $K_m^{0.5\,nM}$ = 368 ± 6.4 μM; $V_{max}^{0.5\,nM}$ = 490 ± 22.4 μmol/min/mg and $K_m^{2\,nM}$ = 492 ± 7.2 μM; and $V_{max}^{2\,nM}$ = 309 ± 60.5 μmol/min/mg. The increased K_m and decreased V_{max} values (Sup. Fig. 5B) indicate that ascofuranone inhibits purified rTAO in a mixed-type non-competitive manner with respect to ubiquinol-1.

4. Discussion

The overall goal of the present study was to obtain a highly pure and stable rTAO protein with maximum specific activity which could be used to investigate the kinetic properties of the enzyme. The quality of the purified rTAO obtained in this study has resulted in three important aspects with respect to the structure of AOX namely, the first direct evidence of stoichiometrically bound iron within the diiron center of rTAO, secondly reliable measurements of kinetic parameters and thirdly that a sample of sufficient purity and yield could be produced that has resulted in the formation of crystals [41].

4.1. Overexpression and purification of rTAO

The difficulties in isolating stable AOXs in an active form have hampered the biochemical and structural analyses of the enzyme including identification of its prosthetic groups, tertiary structural analysis and the definition of enzyme kinetic parameters. The present study reports on the overexpression and purification of active rTAO, which has enabled us to study biochemical and protein chemistry properties of this enzyme. The protocol described in this paper results in the purification of large amounts of stable rTAO with high specific activity. Two factors appeared critical to functionally express highly active rTAO. Firstly, the optimization of culture conditions, including culture duration and IPTG concentration, was crucial for the successful overexpression of rTAO with high specific activity. Secondly, activity was maximized when rTAO was purified from *E. coli* inner membranes—activity decreased substantially when it was isolated from an unpurified membrane fraction. Additionally, changing the detergent from OG to DM following solubilization, also appeared important to maximize yield and activity. Purified rTAO produced in this manner retained complete activity for more than 6 months at 4 °C and for more than 1 month at 20 °C. Furthermore, we have also been able to purify *Sauromattum guttatum* rAOX by this procedure showing the universality of the purification protocol (Elliott, C.E., Kido, Y., Kita, K. and Moore, A.L. unpublished observations).

It is anticipated that highly purified and active AOX will open a new direction with respect to the investigation of the structure and reaction mechanisms of AOXs and contribute to further progress on the study of this novel terminal oxidase. Indeed we recently took advantage of the exceptional stability and purity of the rTAO by performing the first FTIR spectroscopic investigation of any diiron protein [32]. Stepwise reduction of the fully oxidized resting state of rTAO revealed two distinct IR redox difference spectra. The first of these, "signal 1", contained clear features that could be assigned to protonation of at least one carboxylate group, further perturbations of carboxylic and histidine residues, bound ubiquinone and a negative band that might arise from a radical in the fully oxidized protein. A second IR redox difference spectrum, "signal 2", appeared more slowly (within approximately 1 h) once signal 1 had been reduced and is quite distinct from the components which comprise signal 1. The exact identity of the components which result in signal 2 await further investigations. Such a study has not previously been possible with AOX preparations because of protein instability at room temperature.

4.2. Prosthetic group analysis

Prosthetic group analysis summarized in Table 2 revealed that in highly stable and purified rTAO there are two equivalents of iron per rTAO monomer with no other metals, including Cu, Mn and Zn, being detected. EPR spectroscopy confirms that the irons are part of a diiron center since an EPR signal at g = 15 could be detected (Fig. 2) when rTAO is reduced by dithionite in the presence of PMS. The fact that this signal can be detected in all AOXs examined to date suggests that the signal is a characteristic signature of AOXs [30,31] and in agreement with mutational analyses [18,25–29] is further confirmation that TAO, similar to AOXs in other organisms, is a diiron carboxylate protein. Furthermore the data summarized in Table 2 revealed that when the protein was either inactivated or denatured iron was released indicating it is essential for TAO activity. Moreover, this data has established biochemically the validity of predicting the presence of a diiron center from amino acid sequence data, not only in AOX but also in other membrane-bound diiron carboxylate proteins including 5-demethoxyquinone hydroxylase (CLK-1/Coq7) (which also has the diiron binding motif EXXH). It is of interest to note that both AOX and CLK-1/Coq7 utilize ubiquinol as substrate and both are involved in respiration [42–44].

4.3. Kinetic analysis

The inclusion of C10E8 in the assay was found to be critical for the kinetic analysis of TAO and the evaluation of inhibitors. In Table 3, we have calculated fundamental kinetic parameters of TAO and compared them to those of *E. coli* cytochrome *bo* oxidase complex and *S. cerevisiae* ubiquinol–cytochrome *c* reductase [45]. These kinetic constants provide a molecular rationale on how the alternative pathway can effectively compete with other terminal oxidases, although caution must be exercised in the interpretation of this data as it is derived from experiments performed under non-physiological conditions and substrates. Nevertheless Table 3 indicates that TAO has a calculated k_{cat} of $415 \pm 19\ s^{-1}$ (on the basis that the purity of rTAO is 95%), which is slightly higher than that of the cytochrome *bo* oxidase complex ($313\ s^{-1}$), yeast ubiquinol–cytochrome *c* reductase ($153\ s^{-1}$) and previous values reported for the plant AOX ($186\ s^{-1}$), but considerably less than that calculated for cytochrome *c* oxidase ($770\ s^{-1}$) [45–48]. Taking into account that the value of the specificity constant (k_{cat}/K_m) of enzymatic reactions is known to be less than $10^9\ M^{-1}\ s^{-1}$ (from the perspective of diffusion limited access of substrates [49]), it is apparent from Table 3 that both cytochrome *bo* oxidase and TAO have quite high and comparable catalytic activities. These values suggest that the activation energy of both quinol oxidase reactions are similar and furthermore that the quinol oxidase activity of TAO is thermodynamically "alternative" to that of the cytochrome *bo* complex. In contrast however, TAO does not appear to compete effectively with the bc_1 complex in terms of specificity constant and, if the plant AOX possesses a similar specificity constant to that of TAO, it would suggest that plant alternative oxidase activity would be severely curtailed unless the conventional respiratory chain is limited either through inhibition (which appears to be the case under 'stressed conditions') or through down regulation as appears to be the case in thermogenic tissues [12,50,51].

Interestingly ubiquinol-2 oxidation by rTAO showed substrate inhibition at concentrations above 100 μM in a manner similar to that observed when the heterodimeric terminal ubiquinol oxidase of *E. coli*, cytochrome *bd* oxidized ubiquinol-2 as substrate [52]. A lower K_m value of ubiquinol-2 than that of ubiquinol-1 might be related not only to its hydrophobicity but also could be a function of the isoprenoid chain. The peculiar kinetics of ubiquinol-2 might be attributed to the following two points; 1) competition for the ubiquinol-2 oxidation site between the substrate and the product, and 2) the presence of inactive intermediates of the enzyme related to the precise catalytic mechanism.

Kinetic analysis of the mechanism of inhibition by the specific TAO inhibitor ascofuranone (Sup. Fig. 5) indicates that it is a mixed-type inhibitor with respect to ubiquinol-1. The discrepancy between the mixed inhibition observed in this report and competitive inhibition as reported in our previous study [36] might be due to the different assay conditions used in the experiments described in this paper. In the previous study, the kinetic parameters were based on apparent values because enzymatic activity was calculated without detergents and hence only low ranges of ubiquinol-1 concentrations (0.01 K_m–0.3 K_m) could be used. In contrast, the kinetic parameters reported in the current study were determined with much higher reliability since in the presence of C10E8, a much wider range of ubiquinol-1 (0.4 K_m–1.7 K_m) could be used.

Table 3
Kinetic parameters of quinol oxidases (with respect to ubiquinol-1).

	K_m (μM)	V_{max} (μmol/min/mg protein)	k_{cat} (s^{-1})	k_{cat}/K_m ($\mu M^{-1}\ s^{-1}$)
TAO[a]	338 ± 23.2	601 ± 27.0	415 ± 19	1.2
Cyt *bo* oxidase[b]	61	–	313	5.2
Ubiquinol-cyt *c* reductase[c]	13	–	220	16.9

The k_{cat} value of cytochrome *c* oxidase is $k_{cat} = 770\ (s^{-1})$ [46].
All the k_{cat} values listed here were obtained by dividing the V_{max} by the concentration of the enzymes (mol/mg protein).
[a] This study.
[b] *E. coli* cytochrome *bo* oxidase as in Sakamoto et al. [47].
[c] Ubiquinol–cytochrome *c* reductase from bovine heart as in Fato et al. [45].

4.4. Unique feature of AOX

AOX is found in various organisms and recent genome database searches have also identified AOX in different phyla of the Animalia kingdom (Mollusca, Nematoda and Chordata) [17]. It has been suggested that since AOX is absent from mammalian tissues TAO could be a chemotherapeutic target, since it functions in the bloodstream form of *T. brucei* as the only terminal oxidase and hence is essential for the survival of trypanosomes [5,6]. As an AOX protein has also been identified in *Cryptosporidium parvum* [53,54], which causes diarrheal disease cryptosporidiosis, and the recombinant *C. parvum* AOX is also sensitive to ascofuranone and as a result suggests that not only could AOX be a potential drug target in a number of parasites but furthermore ascofuranone could be used to treat a number of infections since this compound shows potent, broad-spectrum antimicrobial activity [53].

In addition to this clinical application, there is considerable interest in the unique characteristics of the enzyme since the functions and properties of TAO are clearly distinct from those of other bacterial quinol oxidases. TAO is a cytochrome-independent and cyanide-insensitive quinol oxidase, whereas cytochrome *bo* and *bd* complexes are cytochrome-dependent and cyanide-sensitive quinol oxidases [34,35]. Furthermore, TAO has various other physiological roles in *T. brucei*; the cytochrome and alternative pathways are both active and functional in the procyclic forms [55] in addition to the bloodstream form, thereby possibly providing metabolic flexibility under changing environmental conditions. TAO activity also appears to regulate the expression of one of the major surface coat proteins, GPEET, in the procyclic form [56], and in addition may regulate the observed programmed cell death-like phenomena in the bloodstream forms [57].

5. Conclusions

The primary aim of our research on TAO is to elucidate the interaction between the enzyme and its substrate or inhibitor, which hopefully could act as a structural guide for ongoing drug development. In addition to the knowledge obtained from this study, further studies on the inhibitory kinetics and structure–activity relationship of ascofuranone derivatives, along with mutational analyses of TAO [27,29] and X-ray structure analysis will undoubtedly have considerable implications with respect to our understanding of how the enzyme interacts with its substrate and inhibitors. A three-dimensional structure of TAO with and without ascofuranone should also shed light on the inhibitory mechanism of this potent drug, which according to this study occurs via a mixed-type inhibition. Such further insights about the interaction between ascofuranone and the enzyme will hopefully lead to a more rational design of more potent and safe anti-trypanosomal drugs.

Acknowledgements

This work was supported in part by Grant-in-aid for Young Scientists (B) 21790402 (to YK), Grant-in-Aid for Scientific Research (C) 21590467 (to YY), Creative Scientific Research Grant 18GS0314 (to KK), Grant-in-aid for Scientific Research on Priority Areas 18073004 (to KK) from the Japanese Society for the Promotion of Science, and Targeted Proteins Research Program (to KK) from the

Japanese Ministry of Education, Science, Culture, Sports and Technology (MEXT) and a grant for research to promote the development of anti-AIDS pharmaceuticals from the Japan Health Sciences Foundation (to KK). ALM gratefully acknowledges BBSRC for financial support and with KK the Prime Ministers Initiative 2 (Connect) fund for collaborative twinning.

Appendix A. Supplementary data

Supplementary data associated with this article can be found, in the online version, at doi:10.1016/j.bbabio.2009.12.021.

References

[1] WHO, Control and surveillance of African trypanosomiasis, Report of a WHO Expert Committee, World Health Organ Tech Rep Ser, vol. 881, 1998, pp. 1–114, I–VI.
[2] C.E. Clayton, P. Michels, Metabolic compartmentation in African trypanosomes, Parasitol. Today 12 (1996) 465–471.
[3] F.R. Opperdoes, P. Borst, S. Bakker, W. Leene, Localization of glycerol-3-phosphate oxidase in the mitochondrion and particulate NAD+-linked glycerol-3-phosphate dehydrogenase in the microbodies of the bloodstream form to *Trypanosoma brucei*, Eur. J. Biochem. 76 (1977) 29–39.
[4] A.B. Clarkson Jr., E.J. Bienen, G. Pollakis, R.W. Grady, Respiration of bloodstream forms of the parasite *Trypanosoma brucei brucei* is dependent on a plant-like alternative oxidase, J. Biol. Chem. 264 (1989) 17770–17776.
[5] M. Chaudhuri, R.D. Ott, G.C. Hill, Trypanosome alternative oxidase: from molecule to function, Trends Parasitol. 22 (2006) 484–491.
[6] C. Nihei, Y. Fukai, K. Kita, Trypanosome alternative oxidase as a target of chemotherapy, Biochim. Biophys. Acta 1587 (2002) 234–239.
[7] N. Minagawa, Y. Yabu, K. Kita, K. Nagai, N. Ohta, K. Meguro, S. Sakajo, A. Yoshimoto, An antibiotic, ascofuranone, specifically inhibits respiration and in vitro growth of long slender bloodstream forms of *Trypanosoma brucei brucei*, Mol. Biochem. Parasitol. 84 (1997) 271–280.
[8] Y. Yabu, A. Yoshida, T. Suzuki, C. Nihei, K. Kawai, N. Minagawa, T. Hosokawa, K. Nagai, K. Kita, N. Ohta, The efficacy of ascofuranone in a consecutive treatment on *Trypanosoma brucei brucei* in mice, Parasitol. Int. 52 (2003) 155–164.
[9] Y. Yabu, T. Suzuki, C. Nihei, N. Minagawa, T. Hosokawa, K. Nagai, K. Kita, N. Ohta, Chemotherapeutic efficacy of ascofuranone in *Trypanosoma vivax*-infected mice without glycerol, Parasitol. Int. 55 (2006) 39–43.
[10] M. Chaudhuri, W. Ajayi, S. Temple, G.C. Hill, Identification and partial purification of a stage-specific 33 kDa mitochondrial protein as the alternative oxidase of the *Trypanosoma brucei brucei* bloodstream trypomastigotes, J. Eukaryot. Microbiol. 42 (1995) 467–472.
[11] A.L. Moore, J.N. Siedow, The regulation and nature of the cyanide-resistant alternative oxidase of plant mitochondria, Biochim. Biophys. Acta 1059 (1991) 121–140.
[12] A.L. Moore, M.S. Albury, Further insights into the structure of the alternative oxidase: from plants to parasites, Biochem. Soc. Trans. 36 (2008) 1022–1026.
[13] J.N. Siedow, A.L. Umbach, The mitochondrial cyanide-resistant oxidase: structural conservation amid regulatory diversity, Biochim. Biophys. Acta 1459 (2000) 432–439.
[14] T. Joseph-Horne, D.W. Hollomon, P.M. Wood, Fungal respiration: a fusion of standard and alternative components, Biochim. Biophys. Acta 1504 (2001) 179–195.
[15] A. McDonald, G. Vanlerberghe, Branched mitochondrial electron transport in the Animalia: presence of alternative oxidase in several animal phyla, IUBMB Life 56 (2004) 333–341.
[16] A.E. McDonald, G.C. Vanlerberghe, Alternative oxidase and plastoquinol terminal oxidase in marine prokaryotes of the Sargasso Sea, Gene 349 (2005) 15–24.
[17] A.E. McDonald, G.C. Vanlerberghe, J.F. Staples, Alternative oxidase in animals: unique characteristics and taxonomic distribution, J. Exp. Biol. 212 (2009) 2627–2634.
[18] D.A. Berthold, M.E. Andersson, P. Nordlund, New insight into the structure and function of the alternative oxidase, Biochim. Biophys. Acta 1460 (2000) 241–254.
[19] C. Affourtit, M.S. Albury, P.G. Crichton, A.L. Moore, Exploring the molecular nature of alternative oxidase regulation and catalysis, FEBS Lett. 510 (2002) 121–126.
[20] D.P. Maxwell, Y. Wang, L. McIntosh, The alternative oxidase lowers mitochondrial reactive oxygen production in plant cells, Proc. Natl. Acad. Sci. U. S. A. 96 (1999) 8271–8276.
[21] A.L. Moore, M.S. Albury, P.G. Crichton, C. Affourtit, Function of the alternative oxidase: is it still a scavenger? Trends Plant Sci. 7 (2002) 478–481.
[22] S. Mackenzie, L. McIntosh, Higher plant mitochondria, Plant Cell 11 (1999) 571–586.
[23] J.N. Siedow, A.L. Umbach, A.L. Moore, The active site of the cyanide-resistant oxidase from plant mitochondria contains a binuclear iron center, FEBS Lett. 362 (1995) 10–14.
[24] M.E. Andersson, P. Nordlund, A revised model of the active site of alternative oxidase, FEBS Lett. 449 (1999) 17–22.
[25] M.S. Albury, C. Affourtit, A.L. Moore, A highly conserved glutamate residue (Glu-270) is essential for plant alternative oxidase activity, J. Biol. Chem. 273 (1998) 30301–30305.
[26] M. Chaudhuri, W. Ajayi, G.C. Hill, Biochemical and molecular properties of the *Trypanosoma brucei* alternative oxidase, Mol. Biochem. Parasitol. 95 (1998) 53–68.
[27] W.U. Ajayi, M. Chaudhuri, G.C. Hill, Site-directed mutagenesis reveals the essentiality of the conserved residues in the putative diiron active site of the trypanosome alternative oxidase, J. Biol. Chem. 277 (2002) 8187–8193.
[28] M.S. Albury, C. Affourtit, P.G. Crichton, A.L. Moore, Structure of the plant alternative oxidase. Site-directed mutagenesis provides new information on the active site and membrane topology, J. Biol. Chem. 277 (2002) 1190–1194.
[29] K. Nakamura, K. Sakamoto, Y. Kido, Y. Fujimoto, T. Suzuki, M. Suzuki, Y. Yabu, N. Ohta, A. Tsuda, M. Onuma, K. Kita, Mutational analysis of the *Trypanosoma vivax* alternative oxidase: the $E(X)_6Y$ motif is conserved in both mitochondrial alternative oxidase and plastid terminal oxidase and is indispensable for enzyme activity, Biochem. Biophys. Res. Commun. 334 (2005) 593–600.
[30] D.A. Berthold, N. Voevodskaya, P. Stenmark, A. Graslund, P. Nordlund, EPR studies of the mitochondrial alternative oxidase. Evidence for a diiron carboxylate center, J. Biol. Chem. 277 (2002) 43608–43614.
[31] A.L. Moore, J.E. Carre, C. Affourtit, M.S. Albury, P.G. Crichton, K. Kita, P. Heathcote, Compelling EPR evidence that the alternative oxidase is a diiron carboxylate protein, Biochim. Biophys. Acta 1777 (2008) 327–330.
[32] A. Maréchal, Y. Kido, K. Kita, A.L. Moore, P.R. Rich, Identification of three redox states of recombinant *Trypanosoma brucei* alternative oxidase by FTIR spectroscopy and electrochemistry, J. Biol. Chem. 284 (2009) 31827–31833.
[33] Y. Fukai, H. Amino, H. Hirawake, Y. Yabu, N. Ohta, N. Minagawa, S. Sakajo, A. Yoshimoto, K. Nagai, S. Takamiya, S. Kojima, K. Kita, Functional expression of the ascofuranone-sensitive *Trypanosoma brucei brucei* alternative oxidase in the cytoplasmic membrane of *Escherichia coli*, Comp. Biochem. Physiol. C Pharmacol. Toxicol. Endocrinol. 124 (1999) 141–148.
[34] K. Kita, K. Konishi, Y. Anraku, Terminal oxidases of *Escherichia coli* aerobic respiratory chain. I. Purification and properties of cytochrome b_{562}–o complex from cells in the early exponential phase of aerobic growth, J. Biol. Chem. 259 (1984) 3368–3374.
[35] K. Kita, K. Konishi, Y. Anraku, Terminal oxidases of *Escherichia coli* aerobic respiratory chain. II. Purification and properties of cytochrome b_{558}–d complex from cells grown with limited oxygen and evidence of branched electron-carrying systems, J. Biol. Chem. 259 (1984) 3375–3381.
[36] C. Nihei, Y. Fukai, K. Kawai, A. Osanai, Y. Yabu, T. Suzuki, N. Ohta, N. Minagawa, K. Nagai, K. Kita, Purification of active recombinant trypanosome alternative oxidase, FEBS Lett. 538 (2003) 35–40.
[37] O. Maglio, F. Nastri, V. Pavone, A. Lombardi, W.F. DeGrado, Preorganization of molecular binding sites in designed diiron proteins, Proc. Natl. Acad. Sci. U. S. A. 100 (2003) 3772–3777.
[38] M.P. Hendrich, E. Munck, B.G. Fox, J.D. Lipscomb, Integer-spin Epr studies of the fully reduced methane monooxygenase hydroxylase component, J. Am. Chem. Soc. 112 (1990) 5861–5865.
[39] W.A. van den Berg, A.A. Stevens, M.F. Verhagen, W.M. van Dongen, W.R. Hagen, Overproduction of the prismane protein from *Desulfovibrio desulfuricans* ATCC 27774 in *Desulfovibrio vulgaris* (Hildenborough) and EPR spectroscopy of the [6Fe–6S] cluster in different redox states, Biochim. Biophys. Acta 1206 (1994) 240–246.
[40] M. Hoefnagel, P.R. Rich, Q. Zhang, J.T. Wiskich, Substrate kinetics of the plant mitochondrial alternative oxidase and the effects of pyruvate, Plant Physiol. 115 (1997) 1145–1153.
[41] Y. Kido, T. Shiba, D.K. Inaoka, K. Sakamoto, T. Nara, T. Aoki, T. Honma, A. Tanaka, M. Inoue, S. Matsuoka, A. Moore, S. Harada, K. Kita, Crystallization and preliminary crystallographic analysis of cyanide-insensitive alternative oxidase from *Trypanosoma brucei brucei*, Acta. Crystallogr. Sect. F Struct. Biol. Cryst. Commun, doi:10.1107/S1744309109054062.
[42] H. Miyadera, H. Amino, A. Hiraishi, H. Taka, K. Murayama, H. Miyoshi, K. Sakamoto, N. Ishii, S. Hekimi, K. Kita, Altered quinone biosynthesis in the long-lived clk-1 mutants of *Caenorhabditis elegans*, J. Biol. Chem. 276 (2001) 7713–7716.
[43] P. Stenmark, J. Grunler, J. Mattsson, P.J. Sindelar, P. Nordlund, D.A. Berthold, A new member of the family of di-iron carboxylate proteins. Coq7 (clk-1), a membrane-bound hydroxylase involved in ubiquinone biosynthesis, J. Biol. Chem. 276 (2001) 33297–33300.
[44] D.A. Berthold, P. Stenmark, Membrane-bound diiron carboxylate proteins, Ann. Rev. Plant Biol. 54 (2003) 497–517.
[45] R. Fato, M. Cavazzoni, C. Castelluccio, G. Parenti Castelli, G. Palmer, M. Degli Esposti, G. Lenaz, Steady-state kinetics of ubiquinol–cytochrome *c* reductase in bovine heart submitochondrial particles: diffusional effects, Biochem. J. 290 (1993) 225–236 K.
[46] H. Witt, F. Malatesta, F. Nicoletti, M. Brunori, B. Ludwig, Tryptophan 121 of subunit II is the electron entry site to cytochrome-*c* oxidase in *Paracoccus denitrificans*. Involvement of a hydrophobic patch in the docking reaction, J. Biol. Chem. 273 (1998) 5132–5136.
[47] Sakamoto, H. Miyoshi, M. Ohshima, K. Kuwabara, K. Kano, T. Akagi, T. Mogi, H. Iwamura, Role of the isoprenyl tail of ubiquinone in reaction with respiratory enzymes: studies with bovine heart mitochondrial complex I and *Escherichia coli bo*-type ubiquinol oxidase, Biochemistry 37 (1998) 15106–15113.
[48] M.H.N. Hoefnagel, J.T. Wiskich, S.A. Madgwick, Z. Patterson, W. Oettmeier, P.R. Rich New, Inhibitors of the ubiquinol oxidase of higher plant mitochondria, Eur. J. Biochem. 233 (1995) 531–537.
[49] R.A. Alberty, G.G. Hammes, Application of the theory of diffusion-controlled reactions to enzyme kinetics, J. Phys. Chem. 62 (1958) 154–159.
[50] R. Clifton, A.H. Millar, J. Whelan, Alternative oxidases in Arabidopsis: a comparative analysis of differential expression in the gene family provides new insights into function of non-phosphorylating bypasses, Biochim. Biophys. Acta 1757 (2006) 730–741.
[51] A.M. Wagner, K. Krab, M.J. Wagner, A.L. Moore, Regulation of thermogenesis in flowering Araceae: the role of the alternative oxidase, Biochim. Biophys. Acta 1777 (2008) 993–1000.

[52] K. Sakamoto, H. Miyoshi, K. Takegami, T. Mogi, Y. Anraku, H. Iwamura, Probing substrate binding site of the *Escherichia coli* quinol oxidases using synthetic ubiquinol analogues, J. Biol. Chem. 271 (1996) 29897–29902.
[53] T. Suzuki, T. Hashimoto, Y. Yabu, Y. Kido, K. Sakamoto, C. Nihei, M. Hato, S. Suzuki, Y. Amano, K. Nagai, T. Hosokawa, N. Minagawa, N. Ohta, K. Kita, Direct evidence for cyanide-insensitive quinol oxidase (alternative oxidase) in apicomplexan parasite *Cryptosporidium parvum*: phylogenetic and therapeutic implications, Biochem. Biophys. Res. Commun. 313 (2004) 1044–1052.
[54] C.W. Roberts, F. Roberts, F.L. Henriquez, D. Akiyoshi, B.U. Samuel, T.A. Richards, W. Milhous, D. Kyle, L. McIntosh, G.C. Hill, M. Chaudhuri, S. Tzipori, R. McLeod, Evidence for mitochondrial-derived alternative oxidase in the apicomplexan parasite *Cryptosporidium parvum*: a potential anti-microbial agent target, Int. J. Parasitol. 34 (2004) 297–308.
[55] R. Walker Jr., L. Saha, G.C. Hill, M. Chaudhuri, The effect of over-expression of the alternative oxidase in the procyclic forms of *Trypanosoma brucei*, Mol. Biochem. Parasitol. 139 (2005) 153–162.
[56] E. Vassella, M. Probst, A. Schneider, E. Studer, C.K. Renggli, I. Roditi, Expression of a major surface protein of *Trypanosoma brucei* insect forms is controlled by the activity of mitochondrial enzymes, Mol. Biol. Cell 15 (2004) 3986–3993.
[57] A. Tsuda, W.H. Witola, K. Ohashi, M. Onuma, Expression of alternative oxidase inhibits programmed cell death-like phenomenon in bloodstream form of *Trypanosoma brucei rhodesiense*, Parasitol. Int. 54 (2005) 243–251.

Acta Crystallographica Section F
Structural Biology and Crystallization Communications
ISSN 1744-3091

Crystallization and preliminary crystallographic analysis of cyanide-insensitive alternative oxidase from *Trypanosoma brucei brucei*

Yasutoshi Kido,[a] Tomoo Shiba,[a] Daniel Ken Inaoka,[a] Kimitoshi Sakamoto,[a] Takeshi Nara,[b] Takashi Aoki,[b] Teruki Honma,[c] Akiko Tanaka,[c] Masayuki Inoue,[d] Shigeru Matsuoka,[d] Anthony Moore,[e] Shigeharu Harada[f]* and Kiyoshi Kita[a]*

[a]Department of Biomedical Chemistry, Graduate School of Medicine, The University of Tokyo, Tokyo 113-0033, Japan, [b]Department of Molecular and Cellular Parasitology, Juntendo University School of Medicine, Tokyo 113-8421, Japan, [c]Systems and Structural Biology Center, RIKEN, Tsurumi, Yokohama 230-0045, Japan, [d]Graduate School of Pharmaceutical Sciences, The University of Tokyo, Tokyo 113-0033, Japan, [e]Biochemistry and Biomedical Sciences, School of Life Sciences, University of Sussex, Falmer, Brighton, England, and [f]Department of Applied Biology, Graduate School of Science and Technology, Kyoto Institute of Technology, Kyoto 606-8585, Japan

Correspondence e-mail: harada@kit.ac.jp, kitak@m.u-tokyo.ac.jp

Received 6 September 2009
Accepted 15 December 2009

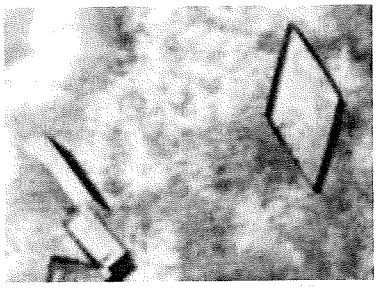

Cyanide-insensitive alternative oxidase (AOX) is a mitochondrial membrane protein and a non-proton-pumping ubiquinol oxidase that catalyzes the four-electron reduction of dioxygen to water. In the African trypanosomes, trypanosome alternative oxidase (TAO) functions as a cytochrome-independent terminal oxidase that is essential for survival in the mammalian host; hence, the enzyme is considered to be a promising drug target for the treatment of trypanosomiasis. In the present study, recombinant TAO (rTAO) overexpressed in haem-deficient *Escherichia coli* was purified and crystallized at 293 K by the hanging-drop vapour-diffusion method using polyethylene glycol 400 as a precipitant. X-ray diffraction data were collected at 100 K and were processed to 2.9 Å resolution with 93.1% completeness and an overall $R_{\rm merge}$ of 9.5%. The TAO crystals belonged to the orthorhombic space group $I222$ or $I2_12_12_1$, with unit-cell parameters a = 63.11, b = 136.44, c = 223.06 Å. Assuming the presence of two rTAO molecules in the asymmetric unit (2 × 38 kDa), the calculated Matthews coefficient ($V_{\rm M}$) was 3.2 Å^3 Da^{-1}, which corresponds to a solvent content of 61.0%. This is the first report of a crystal of the membrane-bound diiron proteins, which include AOXs.

1. Introduction

Cyanide-insensitive respiration in plants has been recognized since the 1920s (Moore & Siedow, 1991). Intensive biochemical studies have revealed that the mitochondrial membrane enzyme alternative oxidase (AOX) is responsible for cyanide-insensitive respiration (Moore & Siedow, 1991; Siedow & Umbach, 2000; Moore & Albury, 2008). AOX, which is cyanide-insensitive and sensitive to salicyl hydroxamic acid (SHAM), is a non-proton-pumping ubiquinol oxidase that catalyzes the four-electron reduction of dioxygen to water (Moore & Albury, 2008). AOX has been found in higher plants, algae, yeast, slime moulds, free-living amoebae, eubacteria and nematodes, as well as in protozoa, including trypanosomes (McDonald *et al.*, 2009).

Trypanosoma brucei, which causes African sleeping sickness in humans and nagana in livestock, which are serious health and economic problems in sub-Saharan Africa (World Health Organization, 2006), is known to show cyanide-insensitive respiration (Opperdoes *et al.*, 1977; Chaudhuri *et al.*, 2006). In the African trypanosomes, trypanosome alternative oxidase (TAO) functions in cyanide-insensitive respiration as a cytochrome-independent terminal oxidase (Clarkson *et al.*, 1989) that is essential for survival in the mammalian host (Clayton & Michels, 1996; Chaudhuri *et al.*, 2006).

TAO is thought to be a good target for antitrypanosomal drugs because mammalian hosts do not possess this protein (Nihei *et al.*, 2002; Chaudhuri *et al.*, 2006). Indeed, we found that ascofuranone, which is isolated from the pathogenic fungus *Ascochyta visiae*, specifically inhibits the quinol oxidase activity of TAO (Minagawa *et al.*, 1997) and rapidly kills the parasites. In addition, we have confirmed the chemotherapeutic efficacy of ascofuranone *in vivo* (Yabu *et al.*, 2003, 2006).

Although TAO and other alternative oxidases (AOXs) contain diiron-binding motifs (E*XX*H) in their amino-acid sequences, their three-dimensional structures have not yet been elucidated (Berthold

& Stenmark, 2003; Moore & Albury, 2008). The high-resolution structure of TAO will undoubtedly have considerable implications with respect to their physicochemical mechanism, enzyme reaction and structure–function relationship, including the interaction between the enzyme and ascofuranone, which may lead to the rational design of more potent and safer antitrypanosomal drugs. Here, we describe the crystallization and preliminary crystallographic analysis of TAO.

2. Materials and methods

2.1. Preparation of rTAO

To construct the host strain FN102 for the expression of rTAO, the Δ*hemA*::Km^R mutation was introduced into *Escherichia coli* strain BL21 (DE3) by P1 transduction as described in a previous study (Nihei *et al.*, 2003). The strain FN102/pTbAO (Nihei *et al.*, 2003) carrying the cDNA for *T. brucei brucei* TAO was precultured at 310 K in 100 ml LB medium (containing 10 mg ampicillin, 5 mg kanamycin and 5 mg 5-aminolevulinic acid) for 4–6 h. The precultured cells were grown aerobically at 303 K in 10 l S-medium [100 g tryptone peptone, 50 g yeast extract, 50 g casamino acids, 104 g K_2HPO_4, 30 g KH_2PO_4, 7.5 g trisodium citrate.$2H_2O$, 25 g $(NH_4)_2SO_4$, 0.5 g $MgSO_4.7H_2O$, 0.25 g $FeSO_4.7H_2O$, 0.25 g $FeCl_3$, 20 g glucose and 0.1 g carbenicillin]. The culture was started at an OD_{600} of 0.01 and expression of His_6-tagged rTAO was induced by the addition of isopropyl β-D-1-thiogalactopyranoside (IPTG; 25 μ*M*) when the OD_{600} reached 0.1. The cells were harvested 8–10 h after induction (about 40 g wet weight). The cells were then resuspended in 200 ml 50 m*M* Tris–HCl pH 7.5 containing 20%(*w*/*w*) sucrose, 0.1 m*M* phenylmethanesulfonylfluoride and protease inhibitor cocktail (Sigma) and broken using a French pressure cell at 200 MPa (Ohtake, Tokyo). Unbroken cells were removed as a pellet by centrifugation at 8000*g* for 10 min (Hitachi 21G). The supernatant (35 ml) was loaded onto 35 ml 50 m*M* Tris–HCl pH 7.5 containing 40%(*w*/*w*) sucrose and ultracentrifuged at 200 000*g* for 1 h at 277 K (Hitachi 85H); the fraction of inner membranes buoyant on the 40%(*w*/*w*) sucrose layer was recovered. The inner-membrane pellet was separated by further ultracentrifugation at 200 000*g* for 1 h (Hitachi 85H) and was resuspended in 30 ml 50 m*M* Tris–HCl pH 7.5 containing 20%(*w*/*w*) sucrose. To solubilize rTAO from the membranes, the membrane suspension (35 ml) was diluted with buffer [50 m*M* Tris–HCl, 200 m*M* $MgSO_4$, 20%(*v*/*v*) glycerol pH 7.3] at 277 K to give a 6 mg ml^{-1} solution and 14%(*w*/*v*) *n*-octyl β-D-glucopyranoside (OG) was added to a final concentration of 1.4%(*w*/*v*). The solution was immediately ultracentrifuged at 200 000*g* for 1 h at 277 K to recover the supernatant containing the solubilized rTAO.

Cobalt-affinity chromatography was performed by a hybrid batch/column procedure using the manufacturer's instructions as stated below. 10 ml BD TALON Metal Affinity Resin (BD Bioscience) equilibrated in a batch format with 100 ml equilibration buffer [20 m*M* Tris–HCl, 1.4%(*w*/*v*) OG, 100 m*M* $MgSO_4$, 20%(*v*/*v*) glycerol pH 7.3] was mixed with 20 ml of the OG extract for 20 min at 277 K. The resin was washed twice with 100 ml of the first wash buffer [20 m*M* Tris–HCl, 20 m*M* imidazole, 0.042%(*w*/*v*) *n*-dodecyl β-D-maltopyranoside (DM), 50 m*M* $MgSO_4$, 20%(*v*/*v*) glycerol pH 7.3] and then transferred to a column for additional washing with 20 ml of the second wash buffer [20 m*M* Tris–HCl, 165 m*M* imidazole, 0.042%(*w*/*v*) DM, 50 m*M* $MgSO_4$, 20%(*v*/*v*) glycerol pH 7.3; flow rate 1 ml min^{-1}]. After washing, rTAO was eluted with elution buffer [20 m*M* Tris–HCl, 200 m*M* imidazole, 0.042%(*w*/*v*) DM, 50 m*M* $MgSO_4$, 60 m*M* NaCl, 20%(*v*/*v*) glycerol pH 7.3; flow rate 1 ml min^{-1}] and the fractions containing rTAO as judged by activity measurements and SDS–PAGE were pooled (Kido *et al.*, 2010).

The fused N-terminal His_6 tag was removed from the purified rTAO using biotinylated thrombin and the tag-free rTAO was separated using streptavidin agarose (Biotinylated Thrombin Cleavage Capture Kit, Novagen) according to the manufacturer's instructions. Incubation with 10 U thrombin for 16 h at 293 K was required for the complete cleavage of 10 mg protein.

The molecular weight of the enzyme in solution was estimated by gel-filtration chromatography using a HiLoad 16/60 Superdex 200 pg column (GE Healthcare). Elution was carried out at a flow rate of 0.3 ml min^{-1} using 50 m*M* Tris–HCl pH 7.4, 0.1 *M* NaCl, 0.042%(*w*/*v*) DM and 20%(*v*/*v*) glycerol.

2.2. Crystallization and X-ray data collection

The purified rTAO was concentrated to 5 mg ml^{-1} in 20 m*M* Tris–HCl, 0.042%(*w*/*v*) DM, 50 m*M* $MgSO_4$, 20%(*v*/*v*) glycerol pH 7.3 using an Amicon Ultra centrifugal filter device (Millipore, 30 kDa molecular-weight cutoff) and used for initial screening of crystallization conditions. Crystallization was performed by the sitting-drop vapour-diffusion technique in 96-well Corning CrystalEX microplates with a conical flat bottom (Hampton Research). In the screening, 0.5 μl rTAO solution was mixed with an equal volume of reservoir solution and the droplet was equilibrated against 100 μl reservoir solution at 277 and 293 K. Commercially available screening kits purchased from Hampton Research (Crystal Screen, Crystal Screen II, Crystal Screen Lite, SaltRx and MembFac), Emerald BioStructures (Wizard I, Wizard II, Cryo I and Cryo II) and Fluidigm (OptiMax-5 Membrane), together with homemade grid-screen reagents containing 100 m*M* buffer (pH 5.0–9.0), 10–40%(*w*/*v*) polyethylene glycol (PEG 400, PEG 1000, PEG 3350, PEG 6000 and PEG 10 000) and 200 m*M* salts (NaCl and KCl), were used as reservoir solutions. However, crystals of rTAO did not appear.

Subsequently, screening was carried out at 277 K using various detergents (DM, OG, *n*-decyl β-D-maltopyranoside, *n*-octyl β-D-maltopyranoside, *n*-nonanoyl *N*-methyl-D-glucamine, octaethylene glycol monododecylether, tetraethylene glycol monooctylether and hexaethylene glycol monodecylether). rTAO samples dissolved in different detergents were subjected to free-interface diffusion in a TOPAZ 8.96 Screening Tip against reservoir solutions purchased from TOPAZ (OptiMax-1, OptiMax-2, OptiMax-3, OptiMax-4 PEG and OptiMax-5 Membrane) using a Fluidigm TOPAZ system (Segelke, 2005). When OG was used as a detergent, several reservoir solutions containing low-molecular-weight PEGs as precipitants gave tiny crystals. The conditions were further optimized by varying the PEG (PEG 200, PEG 400 and PEG 1000) concentration (10–40%), the buffer pH (6.0–8.0), the salt type (48 salts found in PEG/Ion Screen kit from Hampton Research) and the temperature (277 and 293 K) using the sitting-drop vapour-diffusion method. However, crystals larger than 30 μm could not be obtained and moreover they only diffracted X-rays to 7 Å resolution at most.

Next, the effects of additive detergents on crystal growth and X-ray diffraction were examined using reservoir solutions [25–40%(*w*/*v*) PEG 400, 100 m*M* imidazole buffer pH 6.2–7.8 and 200 m*M* potassium formate] supplemented with 0.1–0.5%(*w*/*v*) additive detergents. A dramatic improvement in crystal size was achieved using tetraethylene glycol monooctylether (C8E4) and the conditions, including the concentration of C8E4, were finally optimized.

Currently, crystals with average dimensions of approximately 0.1 × 0.07 × 0.03 mm can be reproducibly obtained at 293 K from reservoir solution consisting of 28–34%(*w*/*v*) PEG 400, 100 m*M*

imidazole buffer pH 7.4, 500 m*M* potassium formate and 0.4%(*w*/*v*) C8E4 using rTAO dissolved in 20 m*M* Tris–HCl pH 7.3, 0.8%(*w*/*v*) OG, 20 m*M* $MgSO_4$ and 20%(*v*/*v*) glycerol.

X-ray diffraction experiments were performed using synchrotron radiation on BL44XU and BL41XU at SPring-8 (Harima, Japan), BL5A and BL17A at Photon Factory and NW12A at Photon Factory Advanced Ring (Tsukuba, Japan). A crystal mounted in a nylon loop was frozen by rapidly submerging it in liquid nitrogen and X-ray diffraction patterns were recorded at 100 K. The best crystals diffracted X-rays to better than 3.0 Å resolution and a total of 180 images were recorded with an oscillation angle of 1°, an exposure time of 5 s per image and a crystal-to-detector distance of 280 mm. The data were processed and scaled using the *HKL*-2000 software package (Otwinowski & Minor, 1997).

3. Results and discussion

His_6-tagged rTAO was solubilized from inner membranes using OG and was purified by cobalt-affinity chromatography in the presence of DM. After removal of the fused N-terminal His_6 tag, about 10 mg of enzyme was obtained from a 10 l culture. The purified rTAO, consisting of 329 amino-acid residues (38 kDa), was >95% pure as estimated by SDS–PAGE (Fig. 1) and its molecular weight in solution was estimated to be 110 kDa by gel-filtration chromatography. As rTAO was prepared as a water-soluble rTAO–DM complex, the complex is probably composed of a homodimer of rTAO with DM molecules bound to the hydrophobic surface of the homodimer. A homodimeric structure of TAO has also been suggested by Chaudhuri *et al.* (2005). The molecular weight of the rTAO–OG complex could not be estimated because elution of rTAO from the gel-filtration column was only successful in the presence of DM as a detergent.

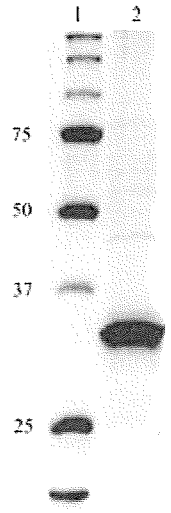

Figure 1
12.5% SDS–PAGE of rTAO with Coomassie Brilliant Blue R-250 staining. Lane 1, molecular-weight markers (kDa); lane 2, rTAO purified by affinity chromatography using BD TALON Metal Affinity Resin.

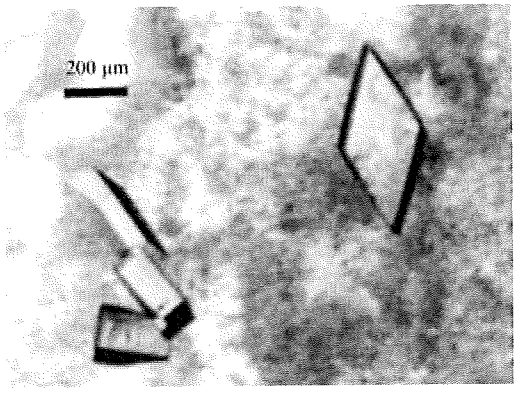

Figure 2
Rhombic plate-shaped crystals of rTAO obtained by the sitting-drop vapour-diffusion method using PEG 400 as a precipitant.

Table 1
Diffraction data statistics.

Values in parentheses are for the outermost resolution shell.

Space group	$I222$ or $I2_12_12_1$
Unit-cell parameters (Å)	a = 63.11, b = 136.44, c = 223.06
Beamline	SPring-8 BL41XU
Wavelength (Å)	1.000
Temperature (K)	100
Resolution (Å)	50.0– 2.90 (2.95–2.90)
Total reflections	135535
Unique reflections	21720
Completeness (%)	93.1 (63.2)
$R_{merge}(I)$† (%)	9.5 (57.3)
$\langle I/\sigma(I)\rangle$	9.8 (1.7)

† $R_{merge}(I) = \sum_{hkl}\sum_i |I_i(hkl) - \langle I(hkl)\rangle| / \sum_{hkl}\sum_i I_i(hkl)$, where $I_i(hkl)$ is the ith measurement of reflection hkl.

After extensive screening and optimization of crystallization conditions, crystals with average dimensions of approximately 0.1 × 0.07 × 0.03 mm could be obtained within 10 d at 293 K using rTAO dissolved in 20 m*M* Tris–HCl pH 7.3, 0.8%(*w*/*v*) OG, 20 m*M* $MgSO_4$ and 20%(*v*/*v*) glycerol with a reservoir solution containing 28–34%(*w*/*v*) PEG 400, 100 m*M* imidazole buffer pH 7.4, 100 m*M* potassium formate and 0.4%(*w*/*v*) C8E4 (Fig. 2).

Analyses of the symmetry and systematic absences in the recorded diffraction patterns indicated that the crystals belonged to the orthorhombic space group $I222$ or $I2_12_12_1$, with unit-cell parameters a = 63.11, b = 136.44, c = 223.06 Å. Assuming the presence of two rTAO molecules in the asymmetric unit (2 × 38 kDa), the calculated Matthews coefficient (V_M) is 3.2 $Å^3\ Da^{-1}$, which corresponds to a solvent content of 61.0%. If the molecular weight of the rTAO–OG complex is presumed to be comparable to that of the rTAO–DM complex, the presence of one molecule of the rTAO–OG complex in the asymmetric unit gives a V_M value of 2.2 $Å^3\ Da^{-1}$ and a solvent content of 44.1%. A data set to 2.9 Å resolution (21 720 unique reflections) was obtained after merging 135 535 reflections recorded on 180 images, with 93.1% completeness and an overall R_{merge} of 9.5%. Statistics of data collection and processing are shown in Table 1. Currently, data collection for phasing using the anomalous dispersion effect of iron is in progress. This is the first report of the crystallization of membrane-bound diiron proteins, which include AOXs.

We thank all staff members of beamlines BL44XU and BL41XU at SPring-8, BL5A and BL17A at Photon Factory and NW12 at Photon Factory Advanced Ring for their help with X-ray diffraction data collection. This work was supported in part by grant-in-aid for Young Scientists (B) 21790402 (to YK), Creative Scientific Research Grant 18GS0314 (to KK), grant-in-aid for Scientific Research on Priority Areas 18073004 (to KK) from the Japanese Society for the Promotion of Science and the Targeted Proteins Research Program (to KK) of the Japanese Ministry of Education, Science, Culture, Sports and Technology (MEXT). ALM gratefully acknowledges the BBSRC for

financial support and, together with KK, the Prime Minister's Initiative 2 (Connect) fund for collaborative twinning.

References

Berthold, D. A. & Stenmark, P. (2003). *Annu. Rev. Plant Biol.* **54**, 497–517.
Chaudhuri, M., Ott, R. D. & Hill, G. C. (2006). *Trends Parasitol.* **22**, 484–491.
Chaudhuri, M., Ott, R. D., Saha, L., Williams, S. & Hill, G. C. (2005). *Parasitol. Res.* **96**, 178–183.
Clarkson, A. B. Jr, Bienen, E. J., Pollakis, G. & Grady, R. W. (1989). *J. Biol. Chem.* **264**, 17770–17776.
Clayton, C. E. & Michels, P. (1996). *Parasitol. Today*, **12**, 465–471.
Kido, Y., Sakamoto, K., Nakamura, K., Harada, M., Suzuki, T., Yabu, Y., Saimoto, H., Yamakura, F., Ohmori, D., Moore, A., Harada, S. & Kita, K., (2010). *Biochim. Biophys. Acta*, doi:10.1016/j.bbabio.2009.12.021.
McDonald, A. E., Vanlerberghe, G. C. & Staples, J. F. (2009). *J. Exp. Biol.* **212**, 2627–2634.
Minagawa, N., Yabu, Y., Kita, K., Nagai, K., Ohta, N., Meguro, K., Sakajo, S. & Yoshimoto, A. (1997). *Mol. Biochem. Parasitol.* **84**, 271–280.
Moore, A. L. & Albury, M. S. (2008). *Biochem. Soc. Trans.* **36**, 1022–1026.
Moore, A. L. & Siedow, J. N. (1991). *Biochim. Biophys. Acta*, **1059**, 121–140.
Nihei, C., Fukai, Y., Kawai, K., Osanai, A., Yabu, Y., Suzuki, T., Ohta, N., Minagawa, N., Nagai, K. & Kita, K. (2003). *FEBS Lett.* **538**, 35–40.
Nihei, C., Fukai, Y. & Kita, K. (2002). *Biochim. Biophys. Acta*, **1587**, 234–239.
Opperdoes, F. R., Borst, P., Bakker, S. & Leene, W. (1977). *Eur. J. Biochem.* **76**, 29–39.
Otwinowski, Z. & Minor, W. (1997). *Methods Enzymol.* **276**, 307–326.
Segelke, B. (2005). *Expert Rev. Proteomics*, **2**, 165–172.
Siedow, J. N. & Umbach, A. L. (2000). *Biochim. Biophys. Acta*, **1459**, 432–439.
World Health Organization (2006). *Wkly Epidemiol. Rec.* **81**, 71–80.
Yabu, Y., Suzuki, T., Nihei, C., Minagawa, N., Hosokawa, T., Nagai, K., Kita, K. & Ohta, N. (2006). *Parasitol. Int.* **55**, 39–43.
Yabu, Y., Yoshida, A., Suzuki, T., Nihei, C., Kawai, K., Minagawa, N., Hosokawa, T., Nagai, K., Kita, K. & Ohta, N. (2003). *Parasitol. Int.* **52**, 155–164.

Mitochondrion 10 (2010) 158–165

Contents lists available at ScienceDirect

Mitochondrion

journal homepage: www.elsevier.com/locate/mito

Contribution of the FAD and quinone binding sites to the production of reactive oxygen species from *Ascaris suum* mitochondrial complex II

Madhavi P. Paranagama [a], Kimitoshi Sakamoto [a,*], Hisako Amino [a], Mutsumi Awano [a], Hideto Miyoshi [b], Kiyoshi Kita [a]

[a] Department of Biomedical Chemistry, Graduate School of Medicine, The University of Tokyo, 7-3-1 Hongo, Bunkyo-ku, Tokyo 113-0033, Japan
[b] Division of Applied Life Sciences, Graduate School of Agriculture, Kyoto University, Sakyo-ku, Kyoto 606-8502, Japan

ARTICLE INFO

Article history:
Received 1 May 2009
Received in revised form 22 October 2009
Accepted 9 December 2009
Available online 16 December 2009

Keywords:
Reactive oxygen species
Complex II
Ascaris suum

ABSTRACT

Reactive oxygen species (ROS) production from mitochondrial complex II (succinate–quinone reductase, SQR) has become a focus of research recently since it is implicated in carcinogenesis. To date, the FAD site is proposed as the ROS producing site in complex II, based on studies done on *Escherichia coli*, whereas the quinone binding site is proposed as the site of ROS production based on studies in *Saccharomyces cerevisiae*. Using the submitochondrial particles from the adult worms and L_3 larvae of the parasitic nematode *Ascaris suum*, we found that ROS are produced from more than one site in the mitochondrial complex II. Moreover, the succinate-dependent ROS production from the complex II of the *A. suum* adult worm was significantly higher than that from the complex II of the L_3 larvae. Considering the conservation of amino acids crucial for the SQR activity and the high levels of ROS production from the mitochondrial complex II of the *A. suum* adult worm together with the absence of complexes III and IV activities in its respiratory chain, it is a good model to examine the reactive oxygen species production from the mitochondrial complex II.

1. Introduction

The complex II superfamily comprises succinate–quinone reductase (SQR) and quinol-fumarate reductase (QFR), which catalyze the interconversion of succinate and fumarate with quinone and quinol. SQR is a component of the aerobic respiratory chain as well as the tricarboxylic acid cycle (for a review see Cecchini et al. (2002)). QFR is a component of the anaerobic respiratory chain in anaerobic and facultative anaerobic bacteria (Lancaster, 2004) and lower eukaryotes (Kita and Takamiya, 2002; Matsumoto et al., 2008; Van Hellmond et al., 2003).

SQR and QFR complexes generally consist of four subunits referred to as the flavoprotein subunit (Fp), iron-sulfur subunit (Ip), cytochrome *b* large subunit (CybL), and cytochrome *b* small subunit (CybS). The Fp and Ip subunits comprise the catalytic domain of the enzyme. The Fp subunit has an FAD as a prosthetic group and contains the dicarboxylate-binding site. The Ip subunit generally contains three iron-sulfur clusters $[2Fe–2S]^{2+,1+}$, $[4Fe–4S]^{2+,1+}$, and $[3Fe–4S]^{1+,0}$. Subunits CybL and CybS, with heme *b* as the prosthetic group, form the anchor domain of the enzyme. This anchors the catalytic domain to the inner mitochondrial membrane and also serves as the quinone oxidation/reduction site (for a review see Cecchini et al. (2002)).

Mutations in the Fp subunit in human complex II result in an infantile onset progressive neurodegenerative disease called Leigh syndrome (Ackrell, 2002; Bourgeron et al., 1995). Mutations in the Ip, CybL, and CybS subunits lead to cancers such as pheochromocytoma (tumours of the chromaffin cells in the adrenal medulla) and paraganglioma (extra adrenal tumours of sympathetic or parasympathetic origin) (Astuti et al., 2001; Bayley et al., 2006; Baysal et al., 2000; Baysal et al., 2002; Eng et al., 2003). Moreover, breast, thyroid, and renal carcinomas are associated with complex II mutations (Ni et al., 2008). However, the precise mechanism associating complex II mutations to carcinogenesis is not fully understood. Currently there are two hypotheses to explain how complex II mutations lead to carcinogenesis. One hypothesis suggests that succinate accumulation resulting from complex II dysfunction leads to stabilization of transcription factor hypoxia-inducible factor-1α (HIF-1α) by inhibiting HIF-1α prolyl hydroxylase (Briere et al., 2005; Cervera et al., 2008; Selak et al., 2005). The other hypothesis suggests that reactive oxygen species (ROS) generated from complex II defect result in oncogenesis (Guzy et al., 2008; Ishii et al., 2005). Thus, the mechanism of ROS generation from complex II has recently

Abbreviations: SQR, succinate:quinone reductase; QFR, quinol:fumarate reductase; SDH, succinate dehydrogenase; FRD, fumarate reductase; ROS, Reactive oxygen species; SOD, superoxide dismutase; SMP, submitochondrial particles.

* Corresponding author. Tel.: +81 3 5841 8202; fax: +81 3 5841 3444.
E-mail addresses: sakamok@m.u-tokyo.ac.jp, ndh1ascaris@yahoo.co.jp (K. Sakamoto).

1567-7249/$ - see front matter © 2009 Elsevier B.V. and Mitochondria Research Society. All rights reserved.
doi:10.1016/j.mito.2009.12.145

become a focus of research. Accumulating evidence indicates that ROS induce neoplasia by mutating nuclear and mitochondrial DNA (Ishii et al., 2005) or by signaling a pseudohypoxic condition by stabilization of the HIF-1α under normoxic conditions (Guzy et al., 2008). To date, the FAD site is proposed as the ROS producing site in complex II, based on studies done on *Escherichia coli* (Messner and Imlay, 2002), whereas the quinone binding site is proposed as the site of ROS production based on studies in *Saccharomyces cerevisiae* (Guo and Lemire, 2003; Szeto et al., 2007).

In adult worms of the parasitic helminth *Ascaris suum*, complex II functions as the terminal oxidase of the anaerobic respiratory chain and catalyzes fumarate reduction (quinol-fumarate reductase; QFR; Kita et al., 2007). Consistent with its physiological function, it shows high fumarate reductase (FRD) activity when the water-soluble dye methyl violegen is used as an artificial electron donor (Amino et al., 2003). Although the adult enzyme shows high FRD activity, the amino acid sequences of all four of its subunits are more similar to the mitochondrial SQR than to the bacterial QFR (Amino et al., 2000; Amino et al., 2003; Kuramochi et al., 1994; Saruta et al., 1995; Saruta et al., 1996). Moreover, the amino acid residues in the FAD binding site and the active site in the catalytic domain as well as the quinone binding site (Q site) are similar to the mitochondrial SQR. In addition, it shows high SQR activity *in vitro* (Iwata et al., 2008; Kita et al., 2002).

During a study of complex II in adult *A. suum*, we found a significant degree of succinate–cytochrome *c* reductase activity in purified *A. suum* adult complex II, even though the preparation did not contain complex III (quinol-cytochrome *c* reductase) (Takamiya et al., 1986). This result raised the possibility that significant electron leak occurred from adult complex II. In the present study, in attempting to verify this possibility, we investigated succinate-dependent ROS production from the parasite's mitochondria. Analysis of submitochondrial particles for superoxide (O_2^-) production using superoxide dismutase inhibitable acetylated cytochrome *c* reduction, and hydrogen peroxide production using catalase inhibitable amplex red oxidation, in the presence and absence of respiratory chain inhibitors, showed the contribution from both the FAD site and Q site of complex II to produce O_2^- and H_2O_2 when succinate is oxidized under aerobic conditions. Considering the conservation of amino acid residues critical for the enzyme reaction between *A. suum* complex II and mitochondrial SQR, our results show that ROS are produced from more than one site in mitochondrial complex II, linked with subtle differences in the amino acid sequences of the enzyme complex.

2. Materials and methods

2.1. Chemicals

Amplex red was obtained from Molecular probes (Eugene, Oregon). Acetylated cytochrome *c*, superoxide dismutase (bovine and *E. coli*), and horseradish peroxidase were from Sigma Chemical Company, USA. Catalase was from Wako, Japan. Atpenin A5 was from Alexis Biochemicals, Switzerland.

2.2. Submitochondrial particles (SMPs)

SMPs were prepared from frozen muscles of *A. suum* adult female worms by the modified method of Matsuno-Yagi and Hatefi (1985). During preparation of mitochondria, Chappell Perry buffer (100 mM KCl, 50 mM Tris–HCl, 1 mM ATP, 5 mM $MgCl_2$ and 1 mM EDTA, pH 7.4) containing 10 mM sodium malonate was used (Yamashita et al., 2004). Mitochondria were subjected to sonication four times for 30 s with 1.5-min intervals (Branson 450 D, Japan) in the same buffer containing 1 mM sodium malonate and $MgCl_2$ and $MnCl_2$ at a final concentration of 10 mM. In addition, the SMP were washed three times in Chappell Perry buffer with 1 mM sodium malonate buffer to remove the ROS scavenging molecules and stored at −80 °C. Mitochondria from L_3 larvae were prepared as previously described (Amino et al., 2003). SMPs were prepared from frozen mitochondria of *A. suum* L_3 larvae by sonicating three times for 30 s with 1.5-min intervals in a water bath sonifier (Sibata Su-25, Model SSC-350H, Japan). They were washed as described in adult SMP preparation and stored at −80 °C. The protein concentration in the SMP samples was estimated by Lowry's method (Lowry et al., 1951), using bovine serum albumin as the standard.

2.3. Superoxide generation assay

The superoxide radical generation rate was assayed using superoxide dismutase (SOD) inhibitable acetylated cytochrome *c* reduction (Azzi et al., 1975; Imlay and Fridovich, 1991; Zhao et al., 2006). The assay was performed in 50 mM potassium phosphate buffer (pH 7.4) containing, 0.25 M sucrose and 1 mM $MgCl_2$ at 25 °C in the presence of 25 μM acetyl cytochrome *c* and 15 μg/ml SMP in a total reaction mixture of 1 ml. After pre-incubating the mixture for 2 min, the reaction was started by adding 0.75 mM sodium succinate or 50 μM NADH. A parallel reaction was run with an additional 30 U/ml superoxide dismutase. The reduction of acetylated cytochrome *c* was monitored spectrophotometrically as the difference in absorbance at 550–540 nm and calculated using the difference in extinction coefficients of ferrocytochrome *c* and ferricytochrome *c*, $\varepsilon^{550-540} = 19\ mM^{-1}\ cm^{-1}$. Non-specific reduction of acetyl cytochrome *c* was excluded by subtracting the amount of cytochrome *c* reduced in the presence of SOD from that in the absence of SOD.

2.4. H_2O_2 generation assay

Oxidation of amplex red (10-acetyl-3,7-dihydroxyphenoxazine) to resorufin was used to assay the H_2O_2 generation rate (Chen et al., 2003; Mohanty et al., 1997; Shinjyo and Kita, 2007). The assay was performed in 50 mM potassium phosphate buffer (pH 7.4) containing, 0.25 M sucrose and 1 mM $MgCl_2$, 50 μmol amplex red, 0.2 U/ml horseradish peroxidase, 15 μg/ml SMP, and 0.75 mM sodium succinate or 50 μM NADH in a total reaction mixture of 1.0 ml maintained at 25 °C. A parallel reaction was run with an additional 1000 U/ml catalase. The resorufin formation rate was monitored spectrophotometrically at 571 nm. The H_2O_2 generation rate was calculated by using a standard curve. Specificity of the reaction was obtained by subtracting the amount of H_2O_2 produced in the presence of catalase from that in the absence of catalase.

In *A. suum* adult SMP, both the O_2^- and H_2O_2 generation assays were also performed in the presence of 10 mM sodium malonate which blocks the dicarboxylate-binding site of complex II; 400 nM atpenin A5, which blocks the Q site of complex II; and 40 nM quinazoline, which blocks the Q site of complex I. In *A. suum* L_3 larval SMP, 10 μM antimycin A (Qi site inhibitor of complex III), 5 μM stigmatellin (Qo site inhibitor of complex III), 5 μM rotenone (Q site inhibitor of complex I) were also employed in the assays. All these inhibitors at the above-mentioned concentrations reduced more than 85% of the corresponding activities.

2.5. Statistical analysis

All the assays were performed in triplicate and the results were expressed as means ± SEM. O_2^- or H_2O_2 production from a particular organism with a given substrate was compared between different experimental conditions using one-way analysis of

variance followed by the Tukey test. The level of significance was $p < 0.05$.

3. Results

3.1. Complex II is the main ROS producing site in the respiratory chain of adult A. suum

Since the presence of antioxidant molecules in the mitochondria interfered with accurate ROS detection, inside-out submitochondrial particles were prepared and washed to eliminate the antioxidant molecules. As shown in Figs. 1a and 1b, substantial production of O_2^- and H_2O_2 was observed from the submitochondrial particles of *A. suum* adults and L_3 larvae. Then, a series of respiratory chain inhibitors in combination with the respiratory substrates were employed in the assays in order to localize the site of ROS production. Quinazoline is a Q site inhibitor of *A. suum* adult complex I (Yamashita et al., 2004) (Fig. 2a). During succinate oxidation, i.e., electron entry into the respiratory chain from complex II, the addition of quinazoline inhibits the reverse flow of electrons into complex I from the quinone pool. As shown in Table 1, quinazoline inhibition did not show a significant effect on succinate-dependent O_2^- production. This result indicates that the contribution of complex I for succinate-dependent ROS production in *A. suum* adult worms is not significant. Since complex III and IV activities are not found in the respiratory chain of adult *A. suum*, the only significant source of O_2^- in its submitochondrial particles must be complex II. Moreover, the addition of quinazoline in the reaction mixture during NADH oxidation, i.e., electron entry from complex I, resulted in 95% suppression of the O_2^- production rate (Table 1) suggesting the possibility of either the Q site of complex I or a redox center/centers in complex II to be the major O_2^- production sites. In order to assess the contribution of the Q site in complex I for O_2^- production, atpenin A5, which inhibits the SQR activity of complex II completely in *A. suum* (Miyadera et al., 2003) (Fig. 2a), was employed. The NADH-dependent O_2^- production rate observed in the presence of atpenin A5 was not significantly different from that in the presence of quinazoline (Table 1), indicating that the Q site of complex I does not contribute to NADH-dependent O_2^- production significantly. The effect of inhibitors on succinate- and NADH-dependent hydrogen peroxide production rates also showed a similar pattern to that of O_2^- (data not shown). Collectively, the above data provide clear evidence to show that complex II is the main ROS producing site in the respiratory chain of *A. suum* adult worms.

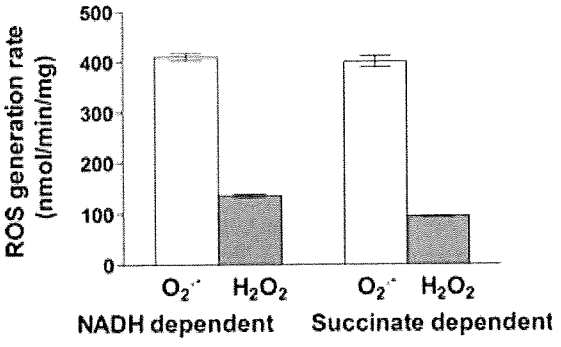

Fig. 1a. Superoxide and hydrogen peroxide generation by SMP of adult *A. suum* worms oxidizing 0.75 mM succinate or 50 μM NADH. Superoxide production was measured as superoxide dismutase inhibitable reduction of acetylated cytochrome *c*, and hydrogen peroxide production was measured as catalase inhibitable oxidation of amplex red as described in Section 2. Results are expressed as means ± SEM of triplicate measurements from three different pools of submitochondrial particles.

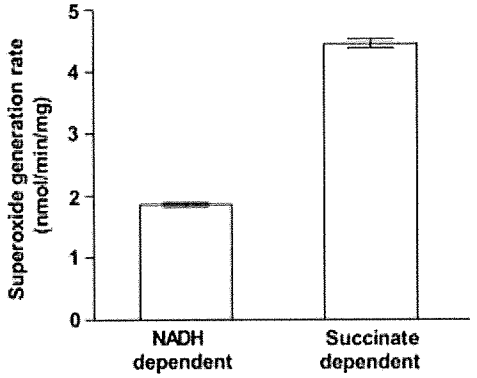

Fig. 1b. Superoxide generation by SMP of *A. suum* L_3 larvae oxidizing 0.5 mM succinate or 50 μM NADH. Superoxide production was measured as superoxide dismutase inhibitable reduction of acetylated cytochrome *c* as described in Section 2. Results are expressed as means ± SEM of triplicate measurements from a single pool of submitochondrial particles. No detectable level of hydrogen peroxide was produced when measured as catalase inhibitable oxidation of amplex red as described in Section 2.

Table 1
Superoxide production from submitochondrial particles of *A. suum* adult worms oxidizing 0.5 mM succinate and 50 μM NADH in the presence of respiratory chain inhibitors. Superoxide production was determined as superoxide dismutase inhibitable reduction of acetylated cytochrome *c* as described in Secton 2. Values are given as nmol/min/mg of protein and expressed as means ± SEM from triplicate measurements on one pool of submitochondrial particles. The decrease of superoxide production (%) in the presence of the inhibitor compared to that in the absence of the inhibitor is given in parentheses.

	Succinate	NADH
No inhibitor	400 ± 11	410 ± 7.75
Quinazoline (40 nM)	359 ± 12 (−10%)	21.1 ± 1.01[b] (−95%)
Atpenin A5 (400 nM)	246 ± 5[a] (−38%)	24.0 ± 0.58[b] (−94%)
Malonate (10 mM)	ND[d]	67.8 ± 4.21[c] (−83%)

[a,b,c] Significantly different from the measurement without an inhibitor. $p < 0.05$.
There was no significant difference between [b]$p < 0.05$.
There was a significant difference between [b]and [c]$p < 0.05$.
[d] ND: not detectable.

3.2. ROS production from the respiratory chain of A. suum L_3 larvae

In *A. suum* L_3 larvae, components of the respiratory chain are similar to those of mammalian mitochondria (Kita and Takamiya, 2002), and complex II serves as SQR. Since the subunit composition of L_3 larvae complex II is different from that of the adult worm (Amino et al., 2000; Amino et al., 2003), succinate- and NADH-dependent ROS production from the SMP of L_3 larvae was also measured in the presence of 5 μM rotenone (Q site inhibitor of complex I), 10 μM antimycin A (Qi site inhibitor of complex III), 5 μM stigmatellin (Qo site inhibitor of complex III), and 10 mM NaN_3 (complex IV inhibitor). In L_3 larvae, the succinate-dependent O_2^- production rate was not significantly affected by the addition of these inhibitors (Table 2). This suggests that complexes I, III, and IV of the L_3 larval respiratory chain do not contribute to O_2^- production during succinate oxidation. Yet, O_2^- production during succinate oxidation was almost completely inhibited by 10 mM malonate and 14% inhibited by atpenin A5. Taken together, these data indicate that complex II is the main succinate-dependent ROS producing site in the submitochondrial particles of *A. suum* L_3 larvae, as is the case for adult worms. On the other hand, malonate and atpenin A5 did not have any effect on NADH-dependent O_2^- production, whereas rotenone significantly increased it. O_2^- production rates in the presence of antimycin A and stigmatellin or NaN_3 were similar to that in the presence of rotenone. These

Table 2
Superoxide production from submitochondrial particles of *A. suum* L_3 larvae oxidizing 0.5 mM succinate or 50 μM NADH in the presence of respiratory chain inhibitors. Superoxide production was determined as superoxide dismutase inhibitable reduction of acetylated cytochrome *c* as described in Section 2. Values are given as nmol/min/mg of protein expressed as means ± SEM from triplicate measurements on one pool of submitochondrial particles. The change of superoxide production (%) in the presence of the inhibitor compared to that in the absence of the inhibitor is given in parentheses.

	Succinate	NADH
No inhibitor	4.45 ± 0.07	1.86 ± 0.03
Rotenone (5 μM)	4.42 ± 0.03 (−0.7%)	2.29 ± 0.07[b] (+23%)
AntimycinA (10 μM)	4.56 ± 0.07 (+3%)	1.62 ± 0.07 (−13%)
Antimycin A (10 μM) + Stigmatellin (5 μM)	4.81 ± 0.03 (+8%)	2.53 ± 0.03[b] (+36%)
NaN_3 (10 mM)	4.87 ± 0 (+9%)	2.63 ± 0.04[b] (+41%)
Malonate (10 mM)	ND[d]	1.62 ± 0.13 (−13%)
Atpenin A5 (400 nM)	3.85 ± 0.07[a] (−14%)	1.82 ± 0.01 (−2%)

[a,b] Significantly different from the measurement without an inhibitor. $p < 0.05$. There was no significant difference among [b] $p < 0.05$.
[d] ND: not detectable.

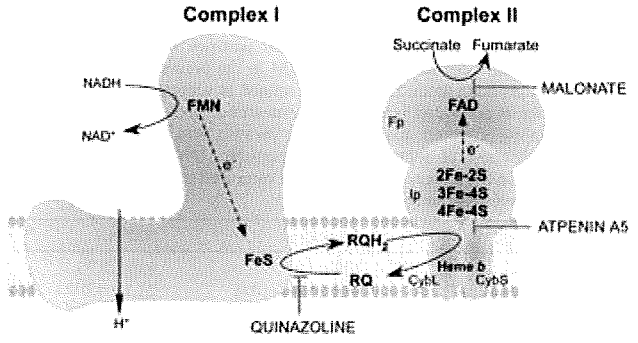

Fig. 2a. Schematic representation of the flow of electrons and the sites of action of inhibitors in the respiratory chain complexes of *A. suum* adult worms.

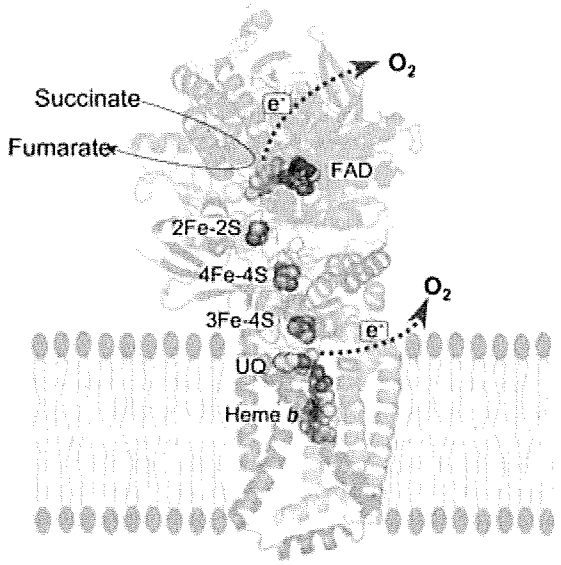

Fig. 2b. Ribbon model of mitochondrial complex II of *S. scrofa* (pdb1ZOY) showing the potential reactive oxygen species production sites identified in *A. suum*. Fp, Ip, CybL and CybS subunits are shown in green, blue, red and orange respectively. The redox centers. FAD, iron-sulfur clusters and heme *b* are as labeled in the figure. Rhodoquinone is supposed to bind to the position of ubiquinone.

observations imply that a redox center in complex I upstream to its Q site is the source of NADH-dependent O_2^- in L_3 larvae. Blocking of complexes III or IV leads to accumulation of electrons at complex I, enhancing the O_2^- production from this site in a similar manner to rotenone. Interestingly, unlike in many mammalian tissues, blocking of the Qi site in complex III did not increase the O_2^- production by submitochondrial particles of L_3 larvae. A quantitative comparison of ROS production between complexes I and II in *A. suum* L_3 larvae showed that the succinate-dependent O_2^- production from complex II is 3-fold higher than NADH-dependent O_2^- production from complex I (Table 2).

3.3. ROS are produced from more than one site in A. suum mitochondrial complex II

In *E. coli*, the flavin of complex IIs is considered to be the source of ROS (Messner and Imlay, 2002). In these enzymes, succinate-dependent ROS production is at a maximum at a lower succinate concentration (at about 1 mM), and at higher succinate concentrations (around 50–100 mM), it is completely inhibited. Hence, excess succinate is suggested to suppress ROS production by hindering the access of oxygen to FAD, thus preventing its autoxidation. When we measured the succinate-dependent ROS production in *A. suum* SMP, it increased with substrate concentration and was highest at 0.5–1 mM succinate in both adults and L_3 larvae (Fig. 3) and gradually decreased along with increasing succinate concentrations. This finding is in accordance with the findings on *E. coli* complex IIs by Messner and Imlay (2002).

However, the percentage of inhibition in ROS production at ⩾100 mM succinate in *A. suum* complex II was only 80%, with 20% always remaining. Further, as shown in Table 1, NADH-dependent O_2^- production was only 83% suppressed by the addition of 10 mM malonate into the reaction mixture. Since malonate is a succinate analogue, which is also known to bind in close proximity to the FAD site in mitochondrial complex II (Huang et al., 2006), it is likely to block the interaction between *A. suum* FAD and oxygen in a manner similar to that in *E. coli* complex IIs, thus decreasing the O_2^- production from the FAD site. Such residual ROS production observed even after complete blocking of the FAD site with succinate or malonate suggests another site for ROS production, in addition to FAD.

The Q site is the other candidate for a potential source of ROS in complex II as reported by Guo and Lemire (2003), and Zhao et al.,

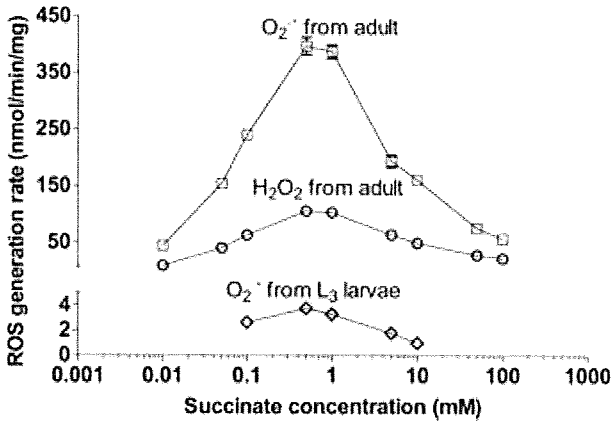

Fig. 3. Effect of succinate concentration on ROS production from *A. suum* SMP. Reaction media for superoxide and hydrogen peroxide measurements were prepared as described in Section 2. Reactions were initiated by addition of succinate at a concentration range of 0.01–100 mM. Points indicate means ± SEM in triplicate measurements from three different pools of SMPs in adult worms and from a single pool in L_3 larvae.

2006. To determine the contribution of the Q site of *A. suum* complex II to ROS production, we analyzed its ROS production in the presence of 400 nM atpenin A5, which inhibits the Q site of complex II completely. O_2^- production from complex II of *A. suum* adult worms with 0.75 mM succinate was decreased 38% in the presence of atpenin A5 (Table 1). In L_3 larvae, it was decreased approximately 14% (Table 2). This observation indicates that binding of atpenin A5 results in reduction in ROS production from *A. suum* complex IIs. In another ROS producing system, xanthine oxidase/hypoxanthine, atpenin A5 interfered with neither ROS production nor detection (data not shown), suggesting that atpenin A5 does not serve as a radical scavenger. Thus, it appears that electrons leak to oxygen from the Q site also during succinate oxidation. Atpenin A5 may inhibit either binding and/or reduction of quinone, thus preventing electron flow in the Q site and inhibiting ROS production.

4. Discussion

Mitochondrial respiratory chain is a significant source of cellular ROS. Impairment of the respiratory chain complexes is known to increase the cellular ROS production (Indo et al., 2007). Historically, complexes I and III are considered as the two major sites of superoxide and hydrogen peroxide production in the respiratory chain (Jezek and Hlavata, 2005; Murphy, 2009; St-Pierre et al., 2002). Interestingly, our results show that complex II is the main site of ROS production in *A. suum* adult respiratory chain (Table 1). In *A. suum* adult respiratory chain, complex II produces equally high amount of superoxide and hydrogen peroxide during the oxidation of the complex I linked substrate NADH and the complex II linked substrate succinate, even under uninhibited conditions (Table 1). This observation is contradictory to the observations so far reported for the mitochondrial respiratory chain in other organisms. Generally, the respiratory chain of isolated mammalian and avian mitochondria and submitochondrial particles respiring under uninhibited conditions produce significant amount of ROS only during succinate oxidation by complex II, but the site of ROS production is not intrinsic to complex II. In this situation, ROS are produced from complex I during the reversed flow of electrons derived from succinate oxidation to reduce NAD (Liu et al., 2002). It is completely abolished by rotenone which inhibits the Q site of complex I (Liu et al., 2002; Muller et al., 2008). One can argue that electrons originating from succinate oxidation in the mitochondrial complex II of *A. suum* adult worm also may flow in the reverse direction through the complex I and leak to oxygen, due to the absence of complexes III and IV activities in its respiratory chain. However, reversed flow of electrons through complex I was not found to be a significant mode of ROS production in the *A. suum* adult respiratory chain since inhibition of the Q site in complex I with quinazoline inhibited only 10% of the succinate-dependent ROS production (Table 1). Another feature of the *A. suum* adult respiratory chain is that it produces significantly high amount of ROS even when the succinate concentration is as low as 10 μM (Fig 3). At such lower concentrations of succinate, detectable level of ROS production is not so far reported from the mitochondrial respiratory chain in other organisms. Similar to our findings, succinate-dependent ROS production intrinsic to complex II was reported from the mitochondrial respiratory chain in *S. cerevisiae* (Guo and Lemire, 2003; Szeto et al., 2007) and *C. elegans* (Senoo-Matsuda et al., 2001; Huang and Lemire, 2009), but the amounts of ROS produced by their complex II were significantly lower than that from *A. suum* adult complex II reported in this study.

It is well established that ROS production is negligible during the oxidation of NADH linked substrates by the uninhibited mitochondrial respiratory chain, but inhibition of the Q site of complex I with an inhibitor such as rotenone results in NADH-dependent ROS production from complex I to a significant level (Hirst et al., 2008). In contrast, addition of the complex I inhibitor quinazoline or the complex II Q site inhibitor aptenin A5 during NADH oxidation in *A. suum* adult SMP almost completely abolished the ROS production detected under uninhibited conditions (Table 1), indicating that complex II is the principal ROS producing site even during NADH oxidation. Thus, our present study shows that *A. suum* adult complex II has the unique feature of significantly high amounts of intrinsic ROS production during oxidation of both the complex I and II linked substrates under uninhibited conditions.

Although it is widely accepted that complex II of the mitochondrial respiratory chain does not have an intrinsic ROS generation under physiological conditions, accumulating evidence indicates that pathogenic mutations in complex II can result in electron leak to oxygen and produce ROS. Simulation of these pathogenic mutations by pharmacological inhibition of complex II activity with thionyl trifluoroacetate (TTFA) (Eto et al., 1992; Guzy et al., 2008) and by genetic inhibition of complex II activity by RNA interference of the Ip subunit (Guzy et al., 2008) has been reported to induce succinate-dependant ROS production, probably due to formation of a flavin radical in the Fp subunit of complex II. In addition, purified and solubilized mitochondrial complex II is also shown to produce ROS through a similar manner (Zhang et al., 1998). Moreover, it has been postulated that ROS may be produced from complex II, if the enzyme is damaged by oxidative stress or ageing also (Jezek and Hlavata, 2005).

Understanding the ROS producing sites in complex II is important in addressing complex II associated diseases linked with ROS production. Currently, there are two models regarding the ROS production site in respiratory chain complex II. One model is based on studies carried out on *E. coli* complex IIs and postulates that the FAD site in the Fp subunit is the principal site of ROS production (Messner and Imlay, 2002; Yankovskaya et al., 2003). Exposure of FAD to the aqueous environment and high electron density are identified as the causes for ROS production from FAD site. This condition is a consequence of interference in electron flow through other redox centers. The other model, based on studies carried out in *S. cerevisiae*, postulates that the ubiquinone-binding site is the major ROS production site. Mutations in Ip, CybL, and CybS subunits are suggested to alter the ubiquinone-binding site, resulting in electron leak (Guo and Lemire, 2003; Szeto et al., 2007).

To gain further insight into ROS production from complex II, we used complex II of the *A. suum* adult worm since it has a high sequence similarity to mitochondrial SQR and produces a significantly high amount of ROS (Fig. 1a). As shown in Table 1, when succinate is utilized as the respiratory substrate, complete inhibition of the Q site of *A. suum* adult respiratory chain with atpenin A5 diminished the level of ROS production by 38%. Since complexes III and IV activities are not detected in *A. suum* adult respiratory chain and the contribution of complex I for succinate-dependent ROS production is not significant (Table 1), this result indicates the possibility of the Q site of the complex II in succinate-dependent ROS generation. The remaining fraction (62%) of the succinate-dependent ROS are likely to be originated from the redox centers located between the Q binding site and the succinate oxidation site in complex II. Those are the Fe-S clusters in the Ip subunit and the FAD site in the Fp subunit. Since Fe-S clusters are buried below the solvent accessible surface of the protein molecule while FAD is localized exposed to the aqueous environment (Sun et al., 2005; Yankovskaya et al., 2003), the probable contributor for the remaining fraction of the ROS appears to be the FAD site. As we have discussed in Section 3.3, the strong suppression of succinate-dependent ROS production at high concentrations of succinate provide evidence for the involvement of FAD site in succinate-dependent ROS production in *A. suum* mitochondrial

complex II. Thus, our data are in accordance with both models of ROS production from complex II (Fig. 2b).

4.1. ROS production from the FAD site

The only other complex II that is so far reported to produce such a high level of ROS from the FAD site is *E. coli* QFR. However, the Fp subunit of *A. suum* adult complex II (QFR) displayed only 37% sequence identity to that of *E. coli* QFR whereas its sequence identity to that of human Fp is much higher (68%). Moreover, the amino acid residues participating in the FAD and dicarboxylate-binding sites in *A. suum* adult complex II are identical to those in the mitochondrial SQR, but not to those in *E. coli* QFR. These observations indicate that the roles of the amino acid residues involved in interacting with FAD and substrate binding in QFR of *E. coli* and *A. suum* are different, although they share in common a high level of FRD activity and ROS production. In contrast, the SQR of *E. coli* has a low level of ROS production (Messner and Imlay, 2002). We also observed a low level of ROS production from complex II in *A. suum* L_3 larvae (Fig. 1b), which has low FRD/SQR activity (0.39) (Amino et al., 2003) despite its high sequence similarity to that of its adult counterpart.

As shown for *E. coli* complex IIs, the principal difference between SQR and QFR lies in the arrangement of redox potentials among the redox centers (Yankovskaya et al., 2003). In *E. coli* QFR, FAD and the 2Fe–2S cluster have the highest redox potentials, thus attracting electrons to fumarate. On the other hand, in *E. coli* SQR, heme *b* and 3Fe–4S have the highest redox potentials, attracting electrons to quinone. These redox potentials are known to be important to drive the electrons in the direction of the physiological reaction of the respective enzymes. Succinate oxidation in SQR and quinol oxidation in QFR leads the enzymes to a reduced state with two electrons. According to theoretical calculations, the distribution of electrons around FAD in the reduced enzyme is 50 times greater in QFR compared to that in SQR in *E. coli* (Yankovskaya et al., 2003). This provides further evidence to the proposal by Messner and Imlay (2002) that the reduced state around FAD is the cause of the high level of ROS production by *E. coli* QFR. Since complex II of *A. suum* adult worms also shows high fumarate reductase activity, it is reasonable to speculate that electrons will sequestrate on its FAD during succinate oxidation with subsequent leak to oxygen.

It appears that, despite the remarkable identity in the amino acid residues interacting with FAD and forming the substrate binding site of *A. suum* adult complex II and mitochondrial SQR, sequestration of electrons on FAD and subsequent leak to oxygen are the features mainly connected to the ability to reduce fumarate by *A. suum* adult complex II. Based on these observations, it is likely that some mutations in mitochondrial SQR may result in accumulation of electrons on FAD and subsequent leakage to oxygen. In fact, it has been shown that mitochondrial complex II produces ROS in pulmonary vasculature due to the reverse flow of electrons under hypoxic conditions (Paddenberg et al., 2003).

4.2. ROS production from the quinone binding site

As shown in Tables 1 and 2, succinate-dependent ROS production from *A. suum* SMP is considerably diminished when the complex II Q site is inhibited with atpenin A5, indicating that the quinone binding site also is a contributor for ROS production from *A. suum* complex II. The quinone binding site is formed by amino acid residues which reside in Ip, CybL, and CybS subunits. Generally, it leaks electrons to oxygen either via a destabilized quinone molecule or directly from the site. To reduce the quinone in complex II completely, two electrons are needed. However, electrons are transferred one at a time from the 3Fe–4S center to the quinone bound at the Q site. Thus, a semiquinone intermediate is an obligatory part of the quinone reduction by complex II. Until another electron arrives, the protein environment of the Q-site donates a proton and stabilizes the semiquinone, thereby preventing its release from the Q site or premature reoxidation. In the latter case, a reduction in the affinity of the Q site for quinone can result in direct transfer of electrons to oxygen from the Q site (Horsefield et al., 2006; Szeto et al., 2007).

As shown by Lemire and colleagues, using the SQR of *S. cerevisiae*, mutations in the amino acid residues associated with quinone binding and reduction lead to high levels of ROS production from the Q site (Guo and Lemire, 2003; Szeto et al., 2007). Yet, except for replacement of Ile C28 with Gly, the amino acid residues important for quinone binding and reduction in SQR enzymes are conserved in *A. suum* adult complex II. Thus, the replacement of Ile C28 to Gly seems to be responsible for ROS production, but this idea is not supported by the sequence of free-living nematode *C. elegans*, which also has Gly in that position without producing significant amounts of ROS. In addition, complex II in *S. cerevisiae*, which has Ser instead of Ile in the corresponding position, also is reported to produce very low amounts of ROS (Guo and Lemire, 2003).

When the conservation of amino acid residues responsible for quinone binding and reduction between mitochondrial SQR and *A. suum* adult complex II, which functions as QFR, are considered together with the high level of ROS production observed only from *A. suum* adult complex II, it appears that differences in the architecture of the quinone binding site caused by subtle differences in its amino acid residues may contribute to the high level of ROS production from its Q site. These differences may result in either an increase in the flow of electrons out of the enzyme or the formation of a destabilized semiquinone radical during quinone reduction, leading to a high degree of ROS production. However, we cannot rule out the possibility of the contribution of rhodoquinone for ROS production from its Q site. Rhodoquinone, which has a lower redox potential (−63 mV) compared to ubiquinone (+110 mV), is a more favorable electron donor to oxygen than ubiquinone (Kita and Takamiya, 2002). In this regard, it is also noteworthy that the Q site in *E. coli* QFR is not known to produce ROS (Messner and Imlay, 2002) despite the presence of menaquinone, which has an even lower redox potential than that of rhodoquinone (−80 mV) (Cecchini et al., 2002). Thus, the presence of a low potential quinone does not appear to be a likely cause of the high level of ROS production from the Q site in *A. suum* adult complex II.

5. Conclusion

We have shown here that under aerobic conditions, both the FAD site and quinone binding site in *A. suum* adult complex II contribute to produce significantly high amounts of O_2^- and H_2O_2 during succinate oxidation, despite its high sequence similarity to mammalian SQR, which does not produce ROS. According to our observations, subtle amino acid differences in complex II subunits may result in leakage of electrons originating from succinate oxidation from more than one site in complex II, forming ROS. Since the amino acids interacting with FAD and participating in succinate binding and quinone reduction in *A. suum* complex II are well conserved, amino acid residues responsible for high reactivity with oxygen may be localized in unique sequences in the parasite's enzyme complex.

In summary, this study shows significant release of ROS from the mitochondrial complex II using the unique *A. suum* model. We believe that *A. suum* adult complex II is a good model to study the mechanism of ROS production from mitochondrial complex II, since amino acid residues conserved among the catalytic domains